

1 **Rapid mass growth and enhanced light extinction of atmospheric aerosols during the heating**
2 **season haze episodes in Beijing revealed by aerosol-chemistry-radiation-boundary layer**
3 **interaction**

4
5 Zhuohui Lin¹, Yonghong Wang^{2,3}, Feixue Zheng¹, Ying Zhou¹, Yishuo Guo¹, Zemin Feng¹, Chang
6 Li¹, Yusheng Zhang¹, Simo Hakala², Tommy Chan², Chao Yan², Kaspar R. Daellenbach², Biwu
7 Chu³, Lubna Dada², Juha Kangasluoma^{1,2}, Lei Yao², Xiaolong Fan¹, Wei Du², Jing Cai², Runlong
8 Cai², Tom V. Kokkonen^{2,4}, Putian Zhou², Lili Wang⁵, Tuukka Petäjä^{2,4}, Federico Bianchi^{1,2}, Veli-
9 Matti Kerminen^{2,4}, Yongchun Liu¹, and Markku Kulmala^{1,2,4}

10

11 ¹Aerosol and Haze Laboratory, Beijing Advanced Innovation Center for Soft Matter Science and
12 Engineering, Beijing University of Chemical Technology, Beijing, China

13 ²Institute for Atmospheric and Earth System Research / Physics, Faculty of Science, University of
14 Helsinki, Finland

15 ³Research Center for Eco-Environmental Sciences, Chinese Academy of Science, Beijing, China

16 ⁴Joint international research Laboratory of Atmospheric and Earth System sciences (JirLATEST),
17 Nanjing University, Nanjing, China

18 ⁵State Key Laboratory of Atmospheric Boundary Layer Physics and Atmospheric Chemistry
19 (LAPC), Institute of Atmospheric Physics, Chinese Academy of Sciences, Beijing 100029, China

20

21

22

23 Corresponding author: Yonghong Wang

24 E-mail: yonghongwang@rcees.ac.cn

25

26 **Abstract**

27

28 Despite the numerous studies investigating haze formation mechanism in China, it is still puzzling
29 that intensive haze episodes could form within hours directly following relatively clean periods.

30 Haze has been suggested to be initiated by the variation of meteorological parameters and then to be
31 substantially enhanced by aerosol-radiation-boundary layer feedback. However, knowledge on the
32 detailed chemical processes and the driving factors for extensive aerosol mass accumulation during
33 the feedback is still scarce. Here, the dependency of the aerosol number size distribution, mass
34 concentration and chemical composition on the daytime mixing layer height (MLH) in urban
35 Beijing is investigated. The size distribution and chemical composition-resolved dry aerosol light
36 extinction is also explored. The results indicate that the aerosol mass concentration and fraction of
37 nitrate increased dramatically when the MLH decreased from high to low conditions, corresponding
38 to relatively clean and polluted conditions, respectively. Particles having their dry diameters in the
39 size of ~400-700 nm, and especially particle-phase ammonium nitrate and liquid water, contributed
40 greatly to visibility degradation during the winter haze periods. The dependency of aerosol
41 composition on the MLH revealed that ammonium nitrate and aerosol water content increased the
42 most during low MLH conditions, which may have further triggered enhanced formation of
43 sulphate and organic aerosol via heterogeneous reactions. As a result, more sulphate, nitrate and
44 water soluble organics were formed, leading to an enhanced water uptake ability and increased light
45 extinction by the aerosols. The results of this study contribute towards a more detailed
46 understanding of the aerosol-chemistry-radiation-boundary layer feedback that is likely to be
47 responsible for explosive aerosol mass growth events in urban Beijing.

48

49

50

51

52

53

54 1. Introduction

55 Despite the recent reduction of air pollutants and their precursors in China between 2013 and 2017,
56 the current emission and air pollution levels are still substantially high (Wang et al., 2020b; Zheng
57 et al., 2018). Such high emissions, combined with specific meteorological conditions, frequently
58 lead to severe haze episodes (An et al., 2019; Wang et al., 2019). Particulate matter, a major air
59 pollutant, has considerable effects on climate, human health and visibility degradation (Che et al.,
60 2007; Lelieveld et al., 2015; Spracklen et al., 2008; Wang et al., 2015).

61
62 During winter haze episodes, a rapid growth of the aerosol mass concentration has commonly been
63 observed, and this phenomenon seems to be directly affected by meteorological factors (Li et al.,
64 2018b; Liu et al., 2018, 2019b; Wang et al., 2018a, 2014a). The meteorological conditions and
65 increased aerosol concentrations are proposed to be interlinked by a feedback loop, called the
66 aerosol-chemistry-boundary layer feedback, in which aerosol particles reduce both solar radiation
67 reaching the surface and turbulent kinetic energy (TKE) of the near-surface air (Ding et al., 2016;
68 Petäjä et al., 2016; Wang et al., 2020d). The reduced TKE owing to aerosol reduce the entrainment
69 of relatively dry air into the mixing layer from above, which makes the air more humid within the
70 mixing layer. The increased relative humidity due to decreased surface temperature enhance the
71 aerosol water uptake ability and promote secondary aerosol formation via aqueous-phase reactions,
72 enhancing light scattering and causing further reduction of solar radiation reaching the surface. All
73 of these factors lead to increased stability of mixing layer height and enhanced air pollution in the
74 mixed layer, which further suppresses the development of boundary layer. As a consequence,
75 concentrations of primary aerosol particles, water vapor and relative humidity increase, creating
76 more favourable conditions for homogeneous and heterogeneous reactions on aerosol surfaces or
77 inside them (Cheng et al., 2016a; Wang et al., 2016; Wu et al., 2018). Such reactions cause rapid
78 formation of secondary aerosol matter and enhanced light extinction during severe winter haze
79 episodes. However, more detailed information on the aerosol and reactive gas chemistry during the
80 aerosol-chemistry-boundary layer feedback and related rapid aerosol mass growth events is still
81 needed (Liu et al., 2019). For instance, it is still unclear which chemical reactions and which

82 compounds in the particulate matter play key roles during such rapid mass growth events.

83

84 The particle number size distribution and chemical composition are considered to be the most
85 important variables influencing the light extinction by aerosol particles. In the atmosphere, the
86 highest contribution to aerosol light extinction comes from organic compounds, nitrate and sulphate
87 in particles with diameters of 100-1000 nm. This is due to the dominant mass fractions of the
88 aforementioned compounds in aerosols that correspond to the peak intensity of solar radiation at
89 wavelengths around 550 nm (Jimenez et al., 2009; Swietlicki et al., 2008). In addition, light
90 scattering which contributes the most to the light extinction by atmospheric aerosols, can be
91 substantially enhanced by the presence of liquid water in the aerosol (Chen et al., 2014; Liu et al.,
92 2019a; Pan et al., 2009; Wang et al., 2020). Hence, quantifying the response of light extinction to
93 different chemical compounds would be helpful in evaluating the feedbacks associated with
94 secondary aerosol production.

95

96 In this study, we focus on the physical and chemical properties of aerosols in Beijing during the
97 winter heating season from October 2018 to February 2019 using state-of-the-art instrumentation.
98 The variation of aerosol chemical composition and the associated light extinction coefficient as a
99 function of the varying mixing layer height are discussed. Our aim is to identify the key chemical
100 components which contribute to the aerosol-chemistry-radiation-boundary layer feedback loop in
101 Beijing.

102

103 **2. Methodology**

104 **2.1. Measurement location and instrumentations**

105 Measurements were conducted between 1 October 2018 and 28 February 2019 at the roof top of the
106 university building at the west campus of Beijing University of Chemical Technology (39.95°N,
107 116.31°E). This station is located about 150 m away from the nearest road (Zizhuyuan road) and

108 500 m away from the West Third Ring Road, and it is surrounded by commercial properties and
109 residential dwellings representative of an urban environment. More details on the location can be
110 found in (Liu et al., 2020; Zhou et al., 2020).

111
112 The meteorological data for this work include basic meteorological variables (relative humidity
113 (RH), temperature, wind speed, wind direction, and visibility) and mixing layer height (MLH)
114 measured using a weather station (Vaisala Inc., Finland) and a Ceilometer CL51 (Vaisala Inc.,
115 Finland), respectively. The MLH is defined as the height above the surface, through which
116 relatively vigorous vertical mixing occurs (Holzworth, 1972), and its value is highly related to the
117 vertical temperature structure and, so some extent, to a mechanically-induced turbulence (Baxter,
118 1991). Here, we followed the method introduced earlier by Münkkel et al. (2007) and Eresmaa et al.
119 (2012) in determining the MLH.

120
121 The number size distributions of aerosol particles from 6 nm to 840 nm were measured by a
122 Differential Mobility Particle Sizer (DMPS) (Aalto et al., 2001). The mass concentration of fine
123 particulate matter (PM_{2.5}) was measured using a Tapered Element Oscillating Microbalance
124 Dichotomous Ambient Particulate Monitor (TEOM 1405-DF, Thermo Fisher Scientific Inc, USA)
125 with a total flow rate of 16.67 L/min (Wang et al., 2014).

126
127 A time-of-flight aerosol chemical speciation monitor (ToF-ACSM, Aerodyne Research Inc.) was
128 used to measure the concentrations of non-refractory (NR) components, including sulfate, nitrate,
129 ammonium, chloride and organics of PM_{2.5} (Fröhlich et al., 2013). A PM_{2.5} cyclone was deployed on
130 the rooftop with a flow rate of 3 L/min. The correlation coefficient of PM_{2.5} measured by TEOM
131 and ToF-ACSM is around 0.9, which indicates the consistence of the two datasets. Aerosol was
132 dried though a Nafion dryer (MD-700-24F-3, PERMA PURE) before entering the ToF- ACSM. The
133 inlet flow was set at 1.4 cm³/s. The particle beam passed through the chamber and reached the
134 heated porous tungsten surface (T≈600°C). There, the non-refractory PM_{2.5} constituents were
135 vaporized and then ionized by electrons (E_{kin}=70eV, emitted by a tungsten filament). The ions were

136 measured by a detector and the data was analyzed using Tofware ver. 2.5.13 within IgorPro ver.
137 6.3.7.2 (WaveMetrics). The relative ionization efficiencies (RIE) for sulfate, nitrate, ammonium,
138 chloride and organics applied were 0.86, 1.05, 4.0, 1.5 and 1.4, respectively. Besides RIE
139 correction, the data also did CO₂+/- NO₃ artifact correction (Pieber et al., 2016) and collection
140 efficiency (CE) correction (Middlebrook et al., 2012). The detailed information has been introduced
141 in Cai et al. (2020). Mass concentrations of ammonium nitrate, ammonium sulfate and ammonium
142 chloride were determined according to the method introduced by Gysel et al. (2007). The aerosol
143 liquid water content (AWC) was calculated by the thermodynamic equilibrium model ISORROPIA
144 II using ToF-ACSM data (Fountoukis and Nenes, 2007).

145 Highly-oxygenated organic molecules (HOMs) were measured by a chemical ionization long time-
146 of-flight mass spectrometer equipped with a nitrate chemical ionization source (LToF-CIMS,
147 Aerodyne Research, Inc. USA) (Jokinen et al., 2012) similar to gas-phase sulfuric acid. The
148 ambient air was drawn into the ionization source through a stainless-steel tube with a length of ~1.6
149 m and a diameter of 3/4 inch at a flowrate of ~ 8 L/min. A 30-40 L/min purified air flow and a 4-8
150 mL/min ultrahigh purity nitrogen flow containing nitric acid were mixed together as the sheath
151 flow, which is guided through a PhotoIonizer (Model L9491, Hamamatsu, Japan) to produce nitrate
152 reagent ions. This sheath flow is then introduced into a co-axial laminar flow reactor concentric to
153 the sample flow. Nitrate ions are pushed to the sample flow layer by an electric field and
154 subsequently charge analytical molecules. Organic carbon (OC) and element carbon (EC)
155 concentrations were measured semi-continuously with a 1-hour time resolution using an OC/EC
156 Analyzer (Model-4, Sunset Lab. Inc.) and time series of ACSM Org and Sunset OC as shown in Fig
157 S6.

158 The ammonia is measured by Trace Ammonia analyzer (Los Gatos Research, Inc.) at atmospheric
159 ambient levels with high precision (0.2 ppb in 1s) and ultra-fast response (5 Hz).

160

161 The air mass history was studied by calculating particle retrorplumes using a Lagrangian particle
162 dispersion model FLEXPART (FLEXible PARTicle dispersion model) ver. 9.02 (Stohl et al., 2005).

163 The ECMWF (European Centre for Medium-Range Weather Forecast) operational forecast (with

164 0.15° horizontal and 1 h temporal resolution) was used as the meteorological input into the model.
165 During the measurement period, a new release of 50 000 test particles, distributed evenly between 0
166 and 100 m above the measurement site, occurred every 1 hour. The released particles were traced
167 backwards in time for 72 h, unless they exceeded the model boundary (20–60°N, 95–135°E).

168

169 2.2. Aerosol light extinction calculation

170 The aerosol light extinction coefficient was calculated with the Mie-Model, which uses particle
171 number size distribution, mass concentrations of different aerosol compounds and their refractive
172 index as inputs (Seinfeld and Pandis, 2006). We introduced a series of assumptions into the Mie-
173 Model, including 1) “internal mixture” which considers each chemical component in a particle as
174 homogeneously mixed with each other; 2) all particles are spherical; and 3) particles of different
175 sizes have the same chemical composition.

176

177 The practical method introduced under those assumptions in previous studies were found to be
178 capable of estimating a variation trend of optical property of PM_{0.5–20} with a relatively good
179 accuracy (Lin et al., 2013).

180

181 Table 1. Summary of the parameters for calculating the average optical refractive index.

182

Species	$\rho_i(\text{g cm}^{-3})$	n_i	k_i
(NH ₄) ₂ SO ₄	1.760	1.530	0.000
NH ₄ NO ₃	1.725	1.554	0.000
NH ₄ Cl	1.527	1.639	0.000
Organics	1.400	1.550	0.001
EC	1.500	1.800	0.540

183

184 The average optical refractive index (AORI) of an internally-mixed particle can be calculated from

185 the optical refractive indices (ORI) of each chemical component by following a mixing rule of
 186 volume-averaged chemical components as $AORI = n_{eff} + k_{eff} \times i$, where the real part (n_{eff}) and
 187 imaginary part (k_{eff}) are given by:

$$n_{eff} = \left(\sum_i n_i \cdot m_i / \rho_i \right) / \left(\sum_i m_i / \rho_i \right) \quad (1)$$

$$k_{eff} = \left(\sum_i k_i \cdot m_i / \rho_i \right) / \left(\sum_i m_i / \rho_i \right) \quad (2)$$

188 Here m_i and ρ_i are the mass concentration and density of the component i in particles,
 189 respectively, and n_i and k_i are the real and imaginary parts of ORI of this component,
 190 respectively. The parameters for calculating the AORI are summarised in Table 1. The values of n_i
 191 and k_i in Table 1 are referenced to the light wavelength of 550 nm.

192

193 $Q_{sp,j}$ represents light scattering efficiency of a single particle with diameter D_j , while $Q_{ep,j}$
 194 represents light absorption efficiency. Theoretically, $Q_{sp,j}$ and $Q_{ep,j}$ are both the function of D_j
 195 and the $AORI_j$ (the AORI of the particle with diameter D_j) at a given light wavelength λ , for
 196 which the complicated calculations were referenced to a previous publication (Lin et al., 2013).
 197 Regarding the limitations of measurement techniques, the $AORI_j$ was assumed to be equal to the
 198 $AORI_{PM2.5}$, which was determined based on chemical composition of $PM_{2.5}$. It is possible to derive
 199 expressions for the cross sections of a spherical particle exactly. The formulas for $Q_{sp,j}$ and $Q_{ep,j}$
 200 are:

201

$$Q_{sp,j}(D_j, \lambda, AORI_j) = \frac{2}{\alpha^2} \sum_{k=1}^{\infty} (2k + 1) \cdot [|a_k|^2 + |b_k|^2] \quad (3)$$

$$Q_{ep,j}(D_j, \lambda, AORI_j) = \frac{2}{\alpha^2} \sum_{k=1}^{\infty} (2k + 1) \cdot Re[a_k + b_k] \quad (4)$$

202

203 where

204

$$a_k = \frac{\alpha \psi'_k(y) \psi_k(\alpha) - y \psi'_k(\alpha) \psi_k(y)}{\alpha \psi'_k(y) \xi_k(\alpha) - y \xi'_k(\alpha) \psi_k(y)}$$

$$b_k = \frac{y \psi'_k(y) \psi_k(\alpha) - \alpha \psi'_k(\alpha) \psi_k(y)}{y \psi'_k(y) \xi_k(\alpha) - \alpha \xi'_k(\alpha) \psi_k(y)}$$

with $y = \alpha m$.

$$m = n_{eff} + i \cdot k_{eff}$$

$$\alpha = \frac{\pi D_j}{\lambda}$$

with $\lambda = 550$ nm.

where complex number m stands for $AOR I_j$, while α is the size of the particle, usually expressed as a dimensionless size parameter. The functions $\psi_k(z)$ and $\xi_k(z)$ are the Riccati–Bessel functions:

$$\psi_k(z) = \left(\frac{\pi z}{2}\right)^{1/2} J_{k+1/2}(z) \quad (5)$$

$$\xi_k(z) = \left(\frac{\pi z}{2}\right)^{1/2} [J_{k+1/2}(z) + i(-1)^k J_{-k-1/2}(z)] \quad (6)$$

where $J_{k+1/2}$ and $J_{-k-1/2}$ are the Bessel functions of the first kind and their footnotes indicate the order of Bessel functions. The Mie theory can serve as the basis of a computational procedure to calculate the scattering and absorption of light by any sphere as a function of wavelength.

According to the Mie-Model, b_{sp} (light scattering coefficient) and b_{ep} (light extinction coefficient) can be quantified with Eqs. (5) and (6), respectively. b_{ap} (light absorption coefficient) is the difference between b_{ep} and b_{sp} , which equals zero, when k_i equals zero or very small. Optical properties including b_{ep} , b_{sp} and b_{ap} to be discussed later are all referenced to light wavelength of 550 nm.

$$b_{sp} = \sum_j b_{sp,j} = \sum_j \frac{\pi D_j^2}{4} \cdot Q_{sp,j}(D_j, \lambda, AORI_j) \cdot N_j \quad (7)$$

$$b_{ep} = \sum_j b_{ep,j} = \sum_j \frac{\pi D_j^2}{4} \cdot Q_{ep,j}(D_j, \lambda, AORI_j) \cdot N_j \quad (8)$$

230

231

232 In Eqs. (7) and (8), D_j stands for the median Stokes diameter in the j -th particle size range and N_j

233 is the number concentration of particles with diameter, D_j .

234

235 3. Results and discussion

3.1. An over of the measurement campaign

The time series particle number size distribution from 6 nm to 840 nm, mass concentrations of nitrate, organics, sulfate, ammonium and chloride in NR_PM_{2.5} (non-refractory PM_{2.5}) and PM_{2.5}, concentration of HOMs and OC are shown in Figure 1(a), (b) and (c). The statistics of these compounds are summarized in Table S1. In general, they showed similar variation patterns (Figure S2 and S3). These concentrations showed high values during haze event than clean days and increased significantly during night time. As shown in Figure 1(b), the rapid mass growth during the heating season in Beijing is related to the rapid growth in nitrate concentration. At the same time, the haze events (PM_{2.5} concentration $\geq 75 \mu\text{g}/\text{m}^3$ and lasting more than one day) are accompanied by particle size growth (Figure 1(a)). To further study which particle size possesses the highest light extinction efficiency during the haze events, and to what extent nitrates contribute to light extinction with the variation of MLH, a case of rapid rapid aerosol mass growth event is selected for further study.

236 **3.2. Typical case of rapid aerosol mass growth episodes affected by aerosol-chemistry-** 237 **boundary layer interactions**

238 An example of rapid aerosol mass growth in urban wintertime Beijing is illustrated in Figure 2,
239 where the haze accumulation was associated with a rapid PM_{2.5} mass concentration increase from
240 8.5 µg/m³ to more than 100 µg/m³ in less than 7 hours. A haze episode started on afternoon 20
241 February 2019 under stagnant meteorological conditions with low wind speeds and elevated
242 ambient relative humidity (Figure S4). The polluted periods during this case occurred under
243 southerly wind transport conditions, whereas clean air masses originated from the north-westerly
244 regions (as shown in Figure S5, S6). These are typical features for a haze evolution process in
245 Beijing (Wang et al., 2020b). During the haze periods marked by the shaded areas in Figure 2, an
246 obvious increase of chemical mass concentration was observed by the ToF-ACSM, characterised by
247 high concentrations of secondary aerosol components (nitrate, organics and sulphate) and typically
248 a shallow boundary layer. The mass concentrations of organics, sulphate and nitrate increased
249 dramatically with a decreasing MLH, accounting for 88.5% of NR-PM_{2.5} during the rapid aerosol
250 mass growth period. The aerosol mass growth was the fastest for nitrate. The mass concentrations of
251 organic and elemental carbon followed that of NR-PM_{2.5}.

252
253 The MLH reached its maximum at around 14:00 in the afternoon of 20 February, after which the
254 development of the mixing layer was suppressed and MLH decreased with the arrival of pollution
255 (Figure 2a). Previous studies have shown that the aerosol-radiation-boundary layer feedback
256 contributes to a rapid enhancement of air pollution (Petäjä et al., 2016; Wang et al., 2020d). High
257 concentrations of aerosol particles obscure downward radiation, as a result of which the surface
258 temperature and sensitive heat flux decrease and the development of mixing layer height is
259 suppressed. Recent studies have gradually realized that the facilitation of various chemical
260 processes play a non-negligible role in the aerosol-radiation-boundary layer feedback (Liu.Q et al.,
261 2018; Liu. Z et al.,2019). Therefore, it is important to identify and quantify the role of different
262 specific chemical species and particle size ranges in reducing atmospheric radiation and extinction.

263

264 Figure 3 shows the contributions of size and chemical composition-resolved dry aerosol to light
265 extinction during the investigated period. As the pollution intensified and MLH decreased (Fig 2c),
266 the light extinction of atmospheric aerosols increased significantly. Assuming that particles of
267 different sizes have the same chemical composition as PM_{2.5} (organics, NH₄NO₃, EC, (NH₄)₂SO₄,
268 NH₄Cl), the light extinction of particles in the size range of 300-700 nm increased significantly
269 from the relative clean period to the polluted period (namely from 12:00 to 16:00). During relatively
270 clean conditions, the contributions of organics, NH₄NO₃, EC, (NH₄)₂SO₄ and NH₄Cl to the total
271 aerosol light extinction were 42%, 23%, 18%, 11% and 7%, respectively. The contribution of
272 NH₄NO₃ to aerosol light extinction reached 40% during the heavily polluted period. Based on the
273 observation it is likely that the increased light extinction by aerosols reduced solar radiation
274 reaching the surface, so that the development of the boundary layer was suppressed.

275

276 **3.3. Connection between the aerosol chemical composition, light extinction, size** 277 **distribution and MLH during the heating season**

278

279 To better characterize the effect of the chemical composition of dry aerosols and the PNSD (particle
280 number size distribution) light extinction under different MLH conditions, the daytime (8:00 –
281 16:00 LT) measurement data from October 2018 to February 2019 were selected for further
282 analysis. As shown by Figure 4 and consistent with other observations in Beijing (Tang et al., 2016;
283 Wang et al., 2020c), there was a general tendency for the PM_{2.5} mass concentration to increase with
284 a decreasing MLH. Organic compounds and nitrate were the most abundant fractions of the daytime
285 aerosol mass composition, contributing together approximately 70% to total NR-PM_{2.5} mass
286 concentration. With a decreasing MLH, the fraction of nitrate mass in NR-PM_{2.5} slightly increased
287 while that of organics decreased. This feature makes the aerosol more hygroscopic under low MLH
288 conditions typical for heavily polluted periods. The increased nitrate fraction in the aerosol could
289 also enhance the formation of other secondary aerosol components (Xue et al., 2019). Note that
290 some fraction of aerosol nitrate could consist of organic nitrate originating from reaction of peroxy

291 radical with nitric oxide; however, it is difficult to distinguish organic nitrate from inorganic nitrate
292 at the moment due to instrumental limitations (Fröhlich et al., 2013).

293

294 Figure 5 depicts the calculated daytime light extinction of the dry aerosol as a function of the MLH,
295 separated by different size ranges and chemical components. We may see that in general, particles
296 with dry diameters in the range of 300-700 nm explains more than 80% of the total aerosol light
297 extinction (Figure 5b). Similar to their share in NR-PM_{2.5}, the fraction of light extinction by
298 ammonium nitrate increased and that of organics decreased during the lowest MLH conditions
299 corresponding to the heavy pollution periods (Figure 5d). There are also apparent differences in the
300 relative contribution of different particle size ranges to light extinction in different MLH conditions:
301 with a decreasing MLH, the contribution of particles with dry diameters larger than about 400-
302 500 nm clearly increased while that of sub-300 nm particles notably decreased. This indicates that
303 the enhanced light extinction by the dry aerosol at low MLH conditions was not only due to the more
304 abundant aerosol mass concentration, but also due to the growth of individual particles to optically
305 more active sizes.

306

307 At relative humidity larger than about 70%, aerosol liquid water gives a significant contribution to
308 the aerosol mass concentration and often a dominant contribution to the aerosol light extinction
309 (Titos et al., 2016). This has important implications for the aerosol-chemistry-radiation-boundary
310 layer feedback, when considering our findings listed above and further noting that heavy pollution
311 periods are often accompanied by high values of RH in Beijing (Zhong et al., 2018). First,
312 compared to clean or moderately-polluted conditions, the enhancement in the aerosol light
313 extinction under polluted is probably much larger than that illustrated in Figure 5. Second, the high
314 aerosol water content under polluted conditions promotes many kinds of chemical reactions taking
315 place on the surface or inside aerosol particles.

316

317 3.4. Aerosol-chemistry-radiation-boundary layer interaction

318

319 In order to further investigate the interaction between MLH and chemical compounds (either
320 observed or calculated), we divided the observed PM_{2.5} concentrations into highly polluted and less
321 polluted conditions using a threshold value of 75 µg /m³ for PM_{2.5}. The organics, nitrate,
322 ammonium, sulfate, chloride, HOM, aerosol water content (AWC) and PM_{2.5} as a function of the
323 mixing layer height during both highly polluted and less polluted conditions are shown in Figure 6.
324 The fitted relationships connecting the concentrations of different chemical compounds to the
325 reduction of MLH under highly and less polluted conditions allowed us to estimate the net mass
326 concentration increase of each compound due to secondary formation and aerosol-chemical-
327 boundary layer feedback under highly polluted conditions (shaded areas in Figure 6). It is worth
328 noting that AWC, nitrate and sulfate increased the most as the MLH decreased, as represented by
329 the large shaded areas in Figs. 6 (h), (b) and (c). The increases of these components are significant
330 as tested (Supplement Information). The day-time nitrate in aerosol is formed predominately via
331 the reaction of nitric acid and ammonium, while nitric acid is produced from gas phase reaction of
332 nitrogen dioxide and hydroxy radical (Seinfeld and Pandis, 2006). High concentrations of daytime
333 nitrate aerosols indicate efficient production of gas phase nitric acid, its partitioning into liquid
334 aerosol and its fast neutralization by abundant ammonia (Li et al., 2018a; Pan et al., 2016; Wang et
335 al., 2020). A recent study shows that condensation of nitric acid and ammonia could promote fast
336 growth of newly formed particle in urban environment condition (Wang et al., 2020d). Another
337 possibility is that ammonium nitrate is formed rapidly on particle surfaces due to the hydrolysis of
338 dinitrogen pentoxide (N₂O₅) during daytime, as the AWC increased significantly (Wang et al.,
339 2014; Wang et al., 2020). However, a quantitative distinction between the two formation pathways
340 for nitrate formation is not possible in this study. The dramatic increase of nitrate aerosol could also
341 promote the formation of sulfate by heterogeneous reactions (Cheng et al., 2016b; Wang et al.,
342 2016). The concentration of HOMs showed a slight increase as the MLH decreased, which suggests
343 that also the formation of HOMs is enhanced with an increased level of air pollution. This
344 phenomenon should be further investigated as HOMs can substantially contribute to the secondary

345 organic aerosol formation.

346

347 Figure 7 displays the dry aerosol light extinction by different chemical compounds in the same way
348 as Figure 6 did for aerosol mass concentrations. The aerosol light extinction is directly related to the
349 reduction of solar radiation reaching the surface, assuming that aerosol chemical components are
350 vertically nearly homogeneously distributed. The light extinction from ammonium nitrate,
351 ammonium sulfate and organics showed significantly increased contributions under highly polluted
352 conditions (low MLH) as compared with less polluted conditions. To the contrary, no such
353 enhancement was observed for ammonium chloride or element carbon (Figs. 7 (d) and (e)). In case
354 of EC this is an expected result, as it originates solely from primary sources. The formation of
355 particle phase chloride have secondary sources from chlorine atom-initiated oxidation of volatile
356 organic compounds, so that the resulting oxidation products could contribute to the observed
357 chloride (Wang and Ruiz, 2017; Wang et al., 2019a).

358

359 To better illustrate the combined effects of secondary aerosol formation and associated feedback on
360 the daytime mass concentrations and light extinction due to different chemical components, we
361 scaled these quantities by either the total PM_{2.5} mass concentration or EC concentration and plotted
362 them as a function of MLH (Fig. 8). With the average level of PM_{2.5} measured by TEOM and ToF-
363 ACSM, the latter scaling minimizes the boundary layer accumulation effect on our analysis, as EC
364 originates from primary emission sources (Cao et al., 2006). As shown in Fig. 8a, organics with
365 their mass fraction of 61% were the most abundant component in PM_{2.5} under high MLH
366 conditions, followed by nitrate and ammonium with their mass fractions of 22% and 13%,
367 respectively. The aerosol was estimated to be rather dry under high MLH conditions ($AWC/PM_{2.5} =$
368 0.03). However, with the decreasing MLH, the fraction of nitrate and the AWC to PM_{2.5} ratio
369 increased up to 45% and 0.2, respectively. This clearly indicates rapid nitrate formation and
370 dramatic increase of the aerosol water uptake from less polluted conditions to intensive haze
371 pollution. Compared with EC (Fig.8c), the concentrations of organic compounds, nitrate, sulfate
372 and ammonium increased by factors of 1.5, 6.3, 4.8 and 4.9 respectively, from the highest to the

373 lowest MLH conditions. Thus, although organics remained as the second most abundant aerosol
374 component after nitrate under haze conditions, secondary formation and associated feedback from
375 less to highly polluted conditions were clearly stronger for both sulfate and ammonium. Efficient
376 sulfate production associated with haze formation has been reported in several studies conducted in
377 China (Cheng et al., 2016; Xie et al., 2015; Xue et al., 2016). Ammonium production during haze
378 formation is tied with neutralization of acidic aerosol by ammonia, which was apparently present
379 abundantly in the gas phase. Compared with the EC concentration, light extinction by (NH₄NO₃)
380 increased the most from the highest MLH conditions (248 M m⁻¹/μg m⁻³) to the lowest MLH
381 conditions (1150 M m⁻¹/μg m⁻³) as shown by Figure 8b. Overall, the rapid growth of nitrate aerosol
382 mass, together with abundant concentration of organic aerosol, were the main cause of the light
383 extinction for dry aerosol under haze formation.

384

385 The mechanism governing the aerosol-chemistry-radiation-boundary layer feedback for the rapid
386 growth of atmospheric aerosol is illustrated in Fig. 9. As a result of reduction in solar radiation and
387 atmospheric heating, a variety of chemical reactions in the gas phase and on particle surfaces or
388 inside them are enhanced with an increased relative humidity and AWC. Such conditions are
389 unfavorable for the dispersion of pollutants, which further enhances atmospheric stability. The
390 formation of hydrophilic compounds, e.g., nitrate, sulfate and oxygenated organic compounds,
391 result in enhanced water uptake by aerosol particles, which will essentially increase heterogeneous
392 reactions associated with these particles. As a result, the aerosol mass and size increase, light
393 extinction is enhanced, and the development of the mixing layer is depressed. At the same time,
394 aerosol precursors concentrated within a shallower mixing layer lead to enhanced production rate of
395 aerosol components in both gas and aerosol phases, especially nitrate but also other secondary
396 aerosol. The increased concentrations of aerosol will further enhance this positive loop.

397

398 **4. Conclusions**

399

400 We investigated the synergetic variations of aerosol chemical composition and mixing layer height
401 during the daytime in urban Beijing. Significant dependency of the sharp increase of ammonium
402 nitrate and aerosol water content with the occurrence of the explosive aerosol mass growth events
403 were observed. We showed that these two components drove a positive aerosol-chemistry-radiation-
404 boundary layer feedback loop, which played an important role in the explosive aerosol mass growth
405 events. A plausible explanation is that the increased aerosol water content at low mixing layer
406 heights provides favorable conditions for heterogeneous reactions for nitrate and sulfate production
407 and neutralization by ammonia. The significant formation of secondary aerosol increases the
408 concentration of aerosol particles in the diameter range 300-700 nm, which effectively reduces the
409 solar radiation reaching the surface and further enhances the aerosol-chemistry-radiation-boundary
410 layer feedback loop. Our analysis connects the aerosol light extinction to a reduction in the mixing
411 layer height, which suppresses the volume into which air pollutants are emitted and leads to an
412 explosive aerosol mass growth. Our results indicate that reduction of ammonium and nitrate
413 concentration in aerosol could weaken the aerosol-radiation-chemistry-boundary layer feedback
414 loop, which could thereby reduce heavy haze episodes in Beijing.

415 **5. Acknowledgements**

416 This work was supported by the funding from Beijing University of Chemical Technology. The
417 European Research Council via advanced grant ATM-GTP (project no. 742206) and Academy of
418 Finland via Academy professor project of M. K.

419 **6. Competing financial interests**

420 The authors declare no competing financial interests.

7. Author contributions

421 YW and MK initiated the study. ZL, YW, FZ, YZ, YG, ZF, CL, YZ, TC, CY, KD, BC, JK, LY, XF,
422 WD, JC and YL conducted the longtime measurements. ZL, YW, LD, RC, SH, PZ, LW, VK, YL

423 and MK interpreted the data. ZL, YW and VK wrote the manuscript.

424

425

426

427

- Aalto, P., Hämeri, K., Becker, E. D. O., Weber, R., Salm, J., Mäkelä, J. M., Hoell, C., O'Dowd, C. D., Karlsson, H., Hansson, H., Väkevä M., Koponen, I. K., Buzorius, G. and Kulmala, M.: Physical characterization of aerosol particles during nucleation events, *Tellus, Series B: Chemical and Physical Meteorology*, 53(4), 344–358, doi:10.3402/tellusb.v53i4.17127, 2001.
- An, Z., Huang, R.-J., Zhang, R., Tie, X., Li, G., Cao, J., Zhou, W., Shi, Z., Han, Y., Gu, Z. and Ji, Y.: Severe haze in northern China: A synergy of anthropogenic emissions and atmospheric processes, *Proceedings of the National Academy of Sciences*, 116(18), 8657 LP – 8666, doi:10.1073/pnas.1900125116, 2019.
- Baxter, R.: Determination of mixing heights from data collected during the 1985 SCCCAMP field program, *Journal of Applied Meteorology*, 30(5), 598–606, doi:10.1175/1520-0450(1991)030<0598:DOMHFD>2.0.CO;2, 1991.
- Cai, J., Chu, B., Yao, L., Yan, C., Heikkinen, L. M., Zheng, F., Li, C., Fan, X., Zhang, S., Yang, D., Wang, Y., Kokkonen, T. V., Chan, T., Zhou, Y., Dada, L., Liu, Y., He, H., Paasonen, P., Kujansuu, J. T., Petäjä, T., Mohr, C., Kangasluoma, J., Bianchi, F., Sun, Y., Croteau, P. L., Worsnop, D. R., Kerminen, V.-M., Du, W., Kulmala, M., and Daellenbach, K. R.: Size-segregated particle number and mass concentrations from different emission sources in urban Beijing, *Atmospheric Chemistry and Physics*, 20, 12721-12740, 10.5194/acp-20-12721-2020, 2020.
- Cao, G., Zhang, X. and Zheng, F.: Inventory of black carbon and organic carbon emissions from China, *Atmospheric Environment*, 40(34), 6516–6527, doi:10.1016/j.atmosenv.2006.05.070, 2006.
- Che, H., Zhang, X., Li, Y., Zhou, Z. and Qu, J. J.: Horizontal visibility trends in China 1981-2005, *Geophysical Research Letters*, 34(24), doi:10.1029/2007GL031450, 2007.
- Chen, J., Zhao, C. S., Ma, N. and Yan, P.: Aerosol hygroscopicity parameter derived from the light scattering enhancement factor measurements in the North China Plain, *Atmos. Chem. Phys*, 14, 8105–8118, doi:10.5194/acp-14-8105-2014, 2014.
- Cheng, Y., Zheng, G., Wei, C., Mu, Q., Zheng, B., Wang, Z., Gao, M., Zhang, Q., He, K., Carmichael, G., Pöschl, U. and Su, H.: Reactive nitrogen chemistry in aerosol water as a source of sulfate during haze events in China, *Science Advances*, 2(12), e1601530–e1601530,

doi:10.1126/sciadv.1601530, 2016b.

Ding, A. J., Huang, X., Nie, W., Sun, J. N., Kerminen, V. M., Petäjä T., Su, H., Cheng, Y. F., Yang, X. Q., Wang, M. H., Chi, X. G., Wang, J. P., Virkkula, A., Guo, W. D., Yuan, J., Wang, S. Y., Zhang, R. J., Wu, Y. F., Song, Y., Zhu, T., Zilitinkevich, S., Kulmala, M. and Fu, C. B.: Enhanced haze pollution by black carbon in megacities in China, *Geophysical Research Letters*, 43(6), 2873–2879, doi:10.1002/2016GL067745, 2016.

Eresmaa, N., Härkönen, J., Joffre, S. M., Schultz, D. M., Karppinen, A. and Kukkonen, J.: A Three-Step Method for Estimating the Mixing Height Using Ceilometer Data from the Helsinki Testbed, *Journal of Applied Meteorology and Climatology*, 51(12), 2172–2187, doi:10.1175/JAMC-D-12-058.1, 2012.

Fountoukis, C. and Nenes, A.: ISORROPIA II: a computationally efficient thermodynamic equilibrium model for

K^+ – Ca^{2+} – Mg^{2+} – NH_4^+ – Na^+ – SO_4^{2-} – NO_3 , *Atmospheric Chemistry and Physics*, 7(17), 4639–4659, doi:10.5194/acp-7-4639-2007, 2007.

Fröhlich, R., Cubison, M. J., Slowik, J. G., Bukowiecki, N., Prévôt, A. S. H., Baltensperger, U., Schneider, J., Kimmel, J. R., Gonin, M., Rohner, U., Worsnop, D. R. and Jayne, J. T.: The ToF-ACSM: A portable aerosol chemical speciation monitor with TOFMS detection, *Atmospheric Measurement Techniques*, 6(11), 3225–3241, doi:10.5194/amt-6-3225-2013, 2013.

Gysel, M., Crosier, J., Topping, D. O., Whitehead, J. D., Bower, K. N., Cubison, M. J., Williams, P. I., Flynn, M. J., McFiggans, G. B. and Coe, H.: Closure study between chemical composition and hygroscopic growth of aerosol particles during TORCH2, *Atmospheric Chemistry and Physics*, 7(24), 6131–6144, doi:10.5194/acp-7-6131-2007, 2007.

Holzworth, G. C.: Mixing heights, wind speeds, and potential for urban air pollution throughout the contiguous united states, , 118, 1972.

Jimenez, J. L., Canagaratna, M. R., Donahue, N. M., Prevot, A. S. H., Zhang, Q., Kroll, J. H., DeCarlo, P. F., Allan, J. D., Coe, H., Ng, N. L., Aiken, A. C., Docherty, K. S., Ulbrich, I. M., Grieshop, A. P., Robinson, A. L., Duplissy, J., Smith, J. D., Wilson, K. R., Lanz, V. A., Hueglin, C., Sun, Y. L., Tian, J., Laaksonen, A., Raatikainen, T., Rautiainen, J., Vaattovaara, P., Ehn, M.,

Kulmala, M., Tomlinson, J. M., Collins, D. R., Cubison, M. J., Dunlea, E. J., Huffman, J. A., Onasch, T. B., Alfarra, M. R., Williams, P. I., Bower, K., Kondo, Y., Schneider, J., Drewnick, F., Borrmann, S., Weimer, S., Demerjian, K., Salcedo, D., Cottrell, L., Griffin, R., Takami, A., Miyoshi, T., Hatakeyama, S., Shimono, A., Sun, J. Y., Zhang, Y. M., Dzepina, K., Kimmel, J. R., Sueper, D., Jayne, J. T., Herndon, S. C., Trimborn, A. M., Williams, L. R., Wood, E. C., Middlebrook, A. M., Kolb, C. E., Baltensperger, U. and Worsnop, D. R.: Evolution of organic aerosols in the atmosphere, *Science*, 326(5959), 1525–1529, doi:10.1126/science.1180353, 2009.

Jokinen, T., Sipilä M., Junninen, H., Ehn, M., Lönn, G., Hakala, J., Petäjä T., Mauldin, R. L., Kulmala, M. and Worsnop, D. R.: Atmospheric sulphuric acid and neutral cluster measurements using CI-API-TOF, *Atmospheric Chemistry and Physics*, 12(9), 4117–4125, doi:10.5194/acp-12-4117-2012, 2012.

Lelieveld, J., Evans, J. S., Fnais, M., Giannadaki, D. and Pozzer, A.: The contribution of outdoor air pollution sources to premature mortality on a global scale, *Nature*, 525(7569), 367–371, doi:10.1038/nature15371, 2015.

Li, H., Zhang, Q., Zheng, B., Chen, C., Wu, N., Guo, H., Zhang, Y., Zheng, Y., Li, X. and He, K.: Nitrate-driven urban haze pollution during summertime over the North China Plain, *Atmospheric Chemistry and Physics*, 18(8), 5293–5306, doi:10.5194/acp-18-5293-2018, 2018a.

Li, J., Sun, J., Zhou, M., Cheng, Z., Li, Q., Cao, X. and Zhang, J.: Observational analyses of dramatic developments of a severe air pollution event in the Beijing area, *Atmospheric Chemistry and Physics*, 18(6), 3919–3935, doi:10.5194/acp-18-3919-2018, 2018b.

Lin, Z. J., Tao, J., Chai, F. H., Fan, S. J., Yue, J. H., Zhu, L. H., Ho, K. F. and Zhang, R. J.: Impact of relative humidity and particles number size distribution on aerosol light extinction in the urban area of Guangzhou, *Atmospheric Chemistry and Physics*, 13(3), 1115–1128, doi:10.5194/acp-13-1115-2013, 2013.

Liu, G., Xin, J., Wang, X., Si, R., Ma, Y., Wen, T., Zhao, L., Zhao, D., Wang, Y. and Gao, W.: Impact of the coal banning zone on visibility in the Beijing-Tianjin-Hebei region, *Science of the Total Environment*, 692, 402–410, doi:10.1016/j.scitotenv.2019.07.006, 2019a.

Liu, Q., Jia, X., Quan, J., Li, J., Li, X., Wu, Y., Chen, D., Wang, Z. and Liu, Y.: New positive

feedback mechanism between boundary layer meteorology and secondary aerosol formation during severe haze events, *Scientific Reports*, 8(1), doi:10.1038/s41598-018-24366-3, 2018.

Liu, Y., Zhang, Y., Lian, C., Yan, C. and Feng, Z.: The promotion effect of nitrous acid on aerosol formation in wintertime Beijing : possible contribution of traffic-related emission, *Atmos. Chem. Phys. Discuss.*, 2020(February), 1–43, doi:10.5194/acp-2020-150, 2020.

Liu, Z., Hu, B., Ji, D., Cheng, M., Gao, W., Shi, S., Xie, Y., Yang, S., Gao, M., Fu, H., Chen, J. and Wang, Y.: Characteristics of fine particle explosive growth events in Beijing, China: Seasonal variation, chemical evolution pattern and formation mechanism, *Science of the Total Environment*, 687, 1073–1086, doi:10.1016/j.scitotenv.2019.06.068, 2019b.

Münkel, C., Eresmaa, N., Räsänen, J. and Karppinen, A.: Retrieval of mixing height and dust concentration with lidar ceilometer, *Boundary-Layer Meteorology*, 124(1), 117–128, doi:10.1007/s10546-006-9103-3, 2007.

Pan, X. L., Yan, P., Tang, J., Ma, J. Z., Wang, Z. F., Gbaguidi, A. and Sun, Y. L.: Observational study of influence of aerosol hygroscopic growth on scattering coefficient over rural area near Beijing mega-city, *Atmospheric Chemistry and Physics*, 9(19), 7519–7530, doi:10.5194/acp-9-7519-2009, 2009.

Pan, Y., Tian, S., Liu, D., Fang, Y., Zhu, X., Zhang, Q., Zheng, B., Michalski, G. and Wang, Y.: Fossil Fuel Combustion-Related Emissions Dominate Atmospheric Ammonia Sources during Severe Haze Episodes: Evidence from ^{15}N -Stable Isotope in Size-Resolved Aerosol Ammonium, *Environmental Science and Technology*, 50(15), 8049–8056, doi:10.1021/acs.est.6b00634, 2016.

Petäjä, T., Järvi, L., Kerminen, V. M., Ding, A. J., Sun, J. N., Nie, W., Kujansuu, J., Virkkula, A., Yang, X., Fu, C. B., Zilitinkevich, S. and Kulmala, M.: Enhanced air pollution via aerosol-boundary layer feedback in China, *Scientific Reports*, 6, doi:10.1038/srep18998, 2016.

Pieber, S. M., El Haddad, I., Slowik, J. G., Canagaratna, M. R., Jayne, J. T., Platt, S. M., Bozzetti, C., Daellenbach, K. R., Fröhlich, R., Vlachou, A., Klein, F., Dommen, J., Miljevic, B., Jimenez, J. L., Worsnop, D. R., Baltensperger, U. and Prévôt, A. S. H.: Inorganic Salt Interference on CO_2^+ in Aerodyne AMS and ACSM Organic Aerosol Composition Studies, *Environmental Science and Technology*, 50(19), 10494–10503, doi:10.1021/acs.est.6b01035, 2016.

Spracklen, D. V., Carslaw, K. S., Kulmala, M., Kerminen, V. M., Sihto, S. L., Riipinen, I., Merikanto, J., Mann, G. W., Chipperfield, M. P., Wiedensohler, A., Birmili, W. and Lihavainen, H.: Contribution of particle formation to global cloud condensation nuclei concentrations, *Geophysical Research Letters*, 35(6), doi:10.1029/2007GL033038, 2008.

Stohl, A., Forster, C., Frank, A., Seibert, P. and Wotawa, G.: Technical note: The Lagrangian particle dispersion model FLEXPART version 6.2, *Atmospheric Chemistry and Physics*, 5(9), 2461–2474, doi:10.5194/acp-5-2461-2005, 2005.

Swietlicki, E., Hansson, H.-C., Hämeri, K., Svenningsson, B., Massling, A., McFiggans, G., McMurry, P. H., Petäjä T., Tunved, P., Gysel, M., Topping, D., Weingartner, E., Baltensperger, U., Rissler, J., Wiedensohler, A. and Kulmala, M.: Hygroscopic properties of submicrometer atmospheric aerosol particles measured with H-TDMA instruments in various environments—a review, *Tellus B: Chemical and Physical Meteorology*, 60(3), 432–469, doi:10.1111/j.1600-0889.2008.00350.x, 2008.

Tang, G., Zhang, J., Zhu, X., Song, T., Münkler, C., Hu, B., Schäfer, K., Liu, Z., Zhang, J., Wang, L., Xin, J., Suppan, P. and Wang, Y.: Mixing layer height and its implications for air pollution over Beijing, China, *Atmos. Chem. Phys.*, 16, 2459–2475, doi:10.5194/acp-16-2459-2016, 2016.

Titos, G., Cazorla, A., Zieger, P., Andrews, E., Lyamani, H., Granados-Muñoz, M. J., Olmo, F. J. and Alados-Arboledas, L.: Effect of hygroscopic growth on the aerosol light-scattering coefficient: A review of measurements, techniques and error sources, *Atmospheric Environment*, 141, 494–507, doi:10.1016/j.atmosenv.2016.07.021, 2016.

Vanhanen, J., Mikkilä J., Lehtipalo, K., Sipilä M., Manninen, H. E., Siivola, E., Petäjä T. and Kulmala, M.: Particle size magnifier for nano-CN detection, *Aerosol Science and Technology*, 45(4), 533–542, doi:10.1080/02786826.2010.547889, 2011.

Wang, G., Zhang, R., Gomez, M. E., Yang, L., Zamora, M. L., Hu, M., Lin, Y., Peng, J., Guo, S., Meng, J., Li, J., Cheng, C., Hu, T., Ren, Y., Wang, Y., Gao, J., Cao, J., An, Z., Zhou, W., Li, G., Wang, J., Tian, P., Marrero-Ortiz, W., Secret, J., Du, Z., Zheng, J., Shang, D., Zeng, L., Shao, M., Wang, W., Huang, Y., Wang, Y., Zhu, Y., Li, Y., Hu, J., Pan, B., Cai, L., Cheng, Y., Ji, Y., Zhang, F., Rosenfeld, D., Liss, P. S., Duce, R. A., Kolb, C. E. and Molina, M. J.: Persistent sulfate

formation from London Fog to Chinese haze, *Proceedings of the National Academy of Sciences of the United States of America*, 113(48), 13630–13635, doi:10.1073/pnas.1616540113, 2016.

Wang, H., Peng, Y., Zhang, X., Liu, H., Zhang, M., Che, H. and Cheng, Y.: Contributions to the explosive growth of PM_{2.5} mass due to aerosol – radiation feedback and decrease in turbulent diffusion during a red alert heavy haze in Beijing – Tianjin – Hebei, China, , 17717–17733, 2018a.

Wang, J., Wang, S., Jiang, J., Ding, A., Zheng, M., Zhao, B., Wong, D. C., Zhou, W., Zheng, G., Wang, L., Pleim, J. E. and Hao, J.: Impact of aerosol-meteorology interactions on fine particle pollution during China's severe haze episode in January 2013, *Environmental Research Letters*, 9(9), doi:10.1088/1748-9326/9/9/094002, 2014a.

Wang, M., Kong, W., Marten, R., He, X.-C., Chen, D., Pfeifer, J., Heitto, A., Kontkanen, J., Dada, L., Kürten, A., Yli-Juuti, T., Manninen, H. E., Amanatidis, S., Amorim, A., Baalbaki, R., Baccharini, A., Bell, D. M., Bertozzi, B., Brüning, S., Brilke, S., Murillo, L. C., Chiu, R., Chu, B., De Menezes, L.-P., Duplissy, J., Finkenzeller, H., Carracedo, L. G., Granzin, M., Guida, R., Hansel, A., Hofbauer, V., Krechmer, J., Lehtipalo, K., Lamkaddam, H., Lampimäki, M., Lee, C. P., Makhmutov, V., Marie, G., Mathot, S., Mauldin, R. L., Mentler, B., Müller, T., Onnela, A., Partoll, E., Petäjä T., Philippov, M., Pospisilova, V., Ranjithkumar, A., Rissanen, M., Rörup, B., Scholz, W., Shen, J., Simon, M., Sipilä M., Steiner, G., Stolzenburg, D., Tham, Y. J., Tomé A., Wagner, A. C., Wang, D. S., Wang, Y., Weber, S. K., Winkler, P. M., Wlasits, P. J., Wu, Y., Xiao, M., Ye, Q., Zauner-Wieczorek, M., Zhou, X., Volkamer, R., Riipinen, I., Dommen, J., Curtius, J., Baltensperger, U., Kulmala, M., Worsnop, D. R., Kirkby, J., Seinfeld, J. H., El-Haddad, I., Flagan, R. C. and Donahue, N. M.: Rapid growth of new atmospheric particles by nitric acid and ammonia condensation, *Nature*, 581(7807), 184–189, doi:10.1038/s41586-020-2270-4, 2020d.

Wang, X., Wang, T., Yan, C., Tham, Y. J., Xue, L., Xu, Z. and Zha, Q.: Large daytime signals of N₂O₅ and NO₃ inferred at 62 amu in a TD-CIMS: Chemical interference or a real atmospheric phenomenon, *Atmospheric Measurement Techniques*, 7(1), 1–12, doi:10.5194/amt-7-1-2014, 2014b.

Wang, Y., Riva, M., Xie, H. and Heikkinen, L.: Formation of highly oxygenated organic molecules from chlorine atom initiated oxidation of alpha-pinene, *Atmospheric Chemistry and Physics*, 2020,

1–31, doi:10.5194/acp-2019-807, 2020.

Wang, Y., Wang, Y., Wang, L., Petäjä T., Zha, Q., Gong, C., Li, S., Pan, Y., Hu, B., Xin, J. and Kulmala, M.: Increased inorganic aerosol fraction contributes to air pollution and haze in China, *Atmos. Chem. Phys.*, 19, 5881–5888, doi:10.5194/acp-19-5881-2019, 2019b.

Wang, Y., Gao, W., Wang, S., Song, T., Gong, Z., Ji, D., Wang, L., Liu, Z., Tang, G., Huo, Y., Tian, S., Li, J., Li, M., Yang, Y., Chu, B., Petäjä T., Kerminen, V.-M., He, H., Hao, J., Kulmala, M., Wang, Y. and Zhang, Y.: Contrasting trends of PM_{2.5} and surface ozone concentrations in China from 2013 to 2017, *National Science Review*, doi:10.1093/nsr/nwaa032, 2020b.

Wang, Y., Chen, Y., Wu, Z., Shang, D., Bian, Y., Du, Z. and Schmitt, S. H.: Mutual promotion between aerosol particle liquid water and particulate nitrate enhancement leads to severe nitrate-dominated particulate matter pollution and low visibility, *Atmos. Chem. Phys.*, (September 2020), 2161–2175, 2020c.

Wang, Y., Yu, M., Wang, Y., Tang, G., Song, T., Zhou, P., Liu, Z., Hu, B., Ji, D., Wang, L., Zhu, X., Yan, C., Ehn, M., Gao, W., Pan, Y., Xin, J., Sun, Y., Kerminen, V.-M., Kulmala, M. and Petäjä T.: Rapid formation of intense haze episodes via aerosol–boundary layer feedback in Beijing, *Atmos. Chem. Phys.*, 20(1), 45–53, doi:10.5194/acp-20-45-2020, 2020d.

Wang, Y. H., Hu, B., Ji, D. S., Liu, Z. R., Tang, G. Q., Xin, J. Y., Zhang, H. X., Song, T., Wang, L. L., Gao, W. K., Wang, X. K. and Wang, Y. S.: Ozone weekend effects in the Beijing-Tianjin-Hebei metropolitan area, China, *Atmos. Chem. Phys.*, 14, 2419–2429, doi:10.5194/acp-14-2419-2014, 2014c.

Wang, Y. H., Liu, Z. R., Zhang, J. K., Hu, B., Ji, D. S., Yu, Y. C. and Wang, Y. S.: Aerosol physicochemical properties and implications for visibility during an intense haze episode during winter in Beijing, *Atmospheric Chemistry and Physics*, 15(6), 3205–3215, doi:10.5194/acp-15-3205-2015, 2015.

Wu, Z., Wang, Y., Tan, T., Zhu, Y., Li, M., Shang, D., Wang, H., Lu, K., Guo, S., Zeng, L. and Zhang, Y.: Aerosol Liquid Water Driven by Anthropogenic Inorganic Salts: Implying Its Key Role in Haze Formation over the North China Plain, *Environmental Science and Technology Letters*, 5(3), 160–166, doi:10.1021/acs.estlett.8b00021, 2018.

Xie, Y., Ding, A., Nie, W., Mao, H., Qi, X., Huang, X., Xu, Z., Kerminen, V. M., Petäjä T., Chi, X., Virkkula, A., Boy, M., Xue, L., Guo, J., Sun, J., Yang, X., Kulmala, M. and Fu, C.: Enhanced sulfate formation by nitrogen dioxide: Implications from in-situ observations at the SORPES station, *Journal of Geophysical Research*, 120(24), 12,679-12,694, doi:10.1002/2015JD023607, 2015.

Xue, J., Yuan, Z., Griffith, S. M., Yu, X., Lau, A. K. H. and Yu, J. Z.: Sulfate Formation Enhanced by a Cocktail of High NO_x, SO₂, Particulate Matter, and Droplet pH during Haze-Fog Events in Megacities in China: An Observation-Based Modeling Investigation, *Environmental Science and Technology*, 50(14), 7325–7334, doi:10.1021/acs.est.6b00768, 2016.

Xue, J., Yu, X., Yuan, Z., Griffith, S. M., Lau, A. K. H., Seinfeld, J. H. and Yu, J. Z.: Efficient control of atmospheric sulfate production based on three formation regimes, *Nature Geoscience*, 12(12), 1–6, doi:10.1038/s41561-019-0485-5, 2019.

Zheng, B., Tong, D., Li, M., Liu, F., Hong, C., Geng, G., Li, H., Li, X., Peng, L., Qi, J., Yan, L., Zhang, Y., Zhao, H., Zheng, Y., He, K. and Zhang, Q.: Trends in China's anthropogenic emissions since 2010 as the consequence of clean air actions, *Atmospheric Chemistry and Physics Discussions*, 1–27, doi:10.5194/acp-2018-374, 2018.

Zhong, J., Zhang, X., Dong, Y., Wang, Y., Liu, C., Wang, J., Zhang, Y. and Che, H.: Feedback effects of boundary-layer meteorological factors on cumulative explosive growth of PM_{2.5} during winter heavy pollution episodes in Beijing from 2013 to 2016, *Atmospheric Chemistry and Physics*, 18(1), 247–258, doi:10.5194/acp-18-247-2018, 2018.

Zhou, Y., Dada, L., Liu, Y., Fu, Y., Kangasluoma, J., Chan, T., Yan, C., Chu, B., Daellenbach, K. R., Bianchi, F., Kokkonen, T. V., Liu, Y., Kujansuu, J., Kerminen, V.-M., Petäjä T., Wang, L., Jiang, J. and Kulmala, M.: Variation of size-segregated particle number concentrations in wintertime Beijing, *Atmospheric Chemistry and Physics*, 20(2), 1201–1216, doi:10.5194/acp-20-1201-2020, 2020.

429

430

431

432

433

434

435

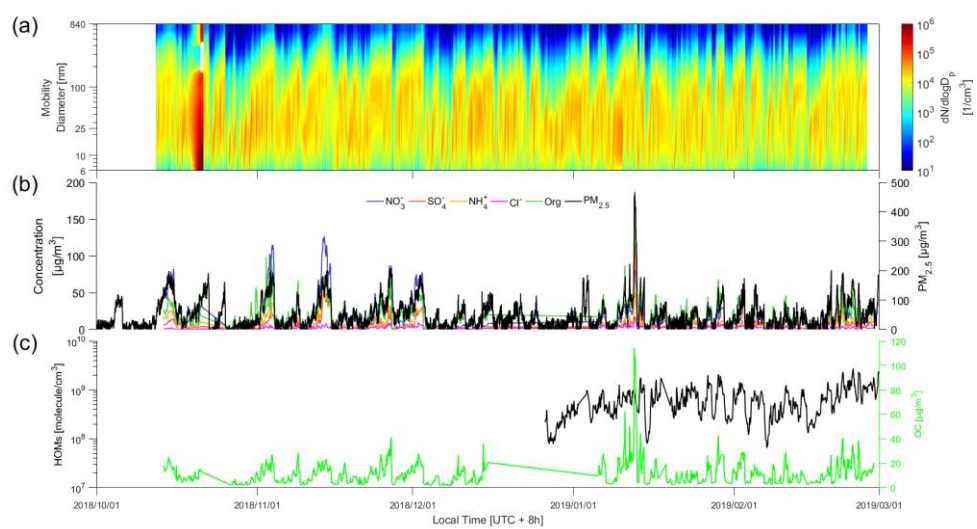
436

437

438

439 Figure caption

440



441

442 Figure 1. Time series of (a) particle number concentration distribution (PNSD) from 6 nm to 840

443 nm (b) chemical composition of NR_PM_{2.5} and PM_{2.5} mass concentrations (c) The concentrations of

444 organic carbon (OC) and highly oxygenated organic molecules (HOM).

445

446

447

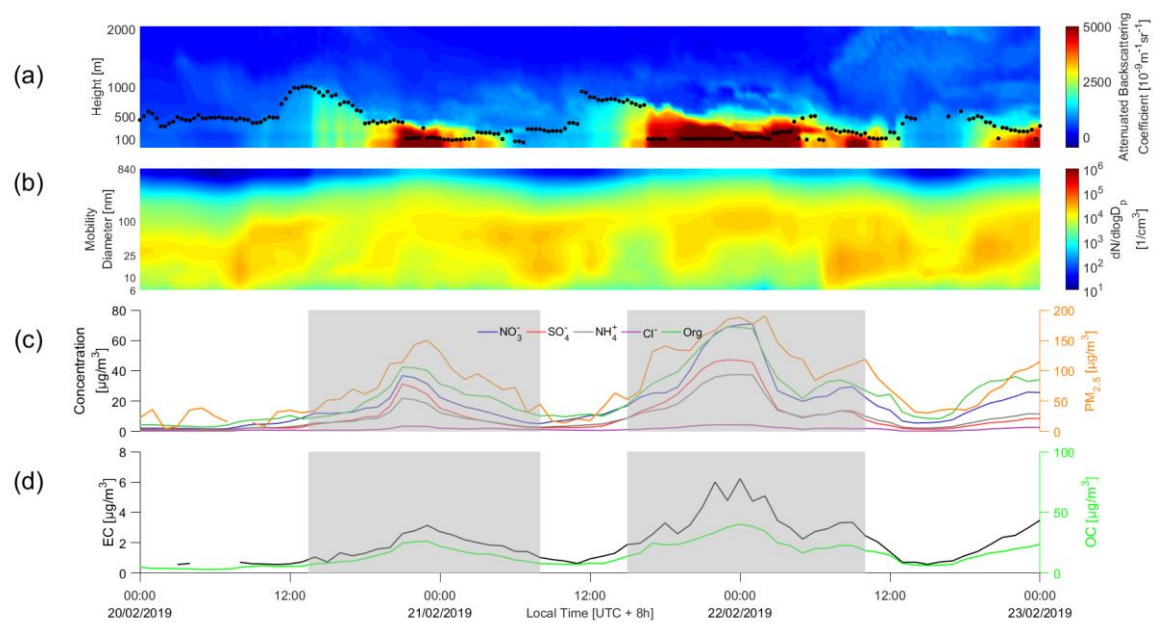
448

449

450

451

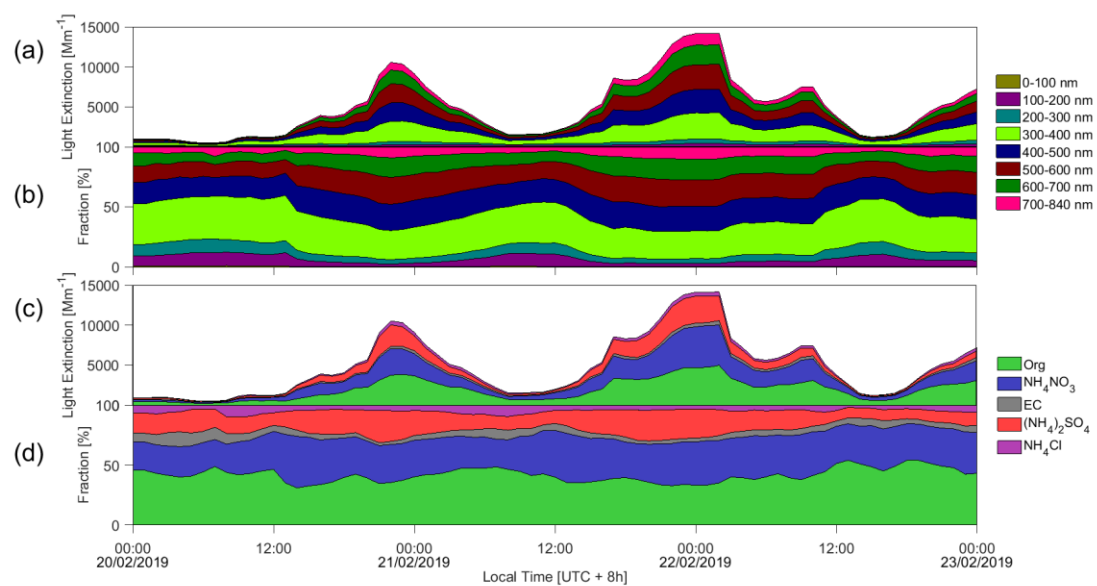
452
453
454
455
456
457
458
459
460
461



462
463
464
465
466
467
468
469
470

Figure 2. Time series of (a) attenuated backscattering coefficient and mixing layer height (b) particle number concentration distribution (PNSD), (c) chemical composition and $\text{PM}_{2.5}$ mass concentrations and (d) elemental carbon (EC) and organic carbon (OC). The haze periods are marked by the shaded areas.

471
472
473
474
475
476
477
478
479



480
481 Figure 3. Time series of (a, b) variation of light extinction from different size aerosol and fractions,
482 and (c, d) variation of light extinction from different aerosol species and fractions. The legends in
483 the left side of figures are particle diameter and the right side are chemical compositions,
484 respectively.

485
486
487
488
489
490

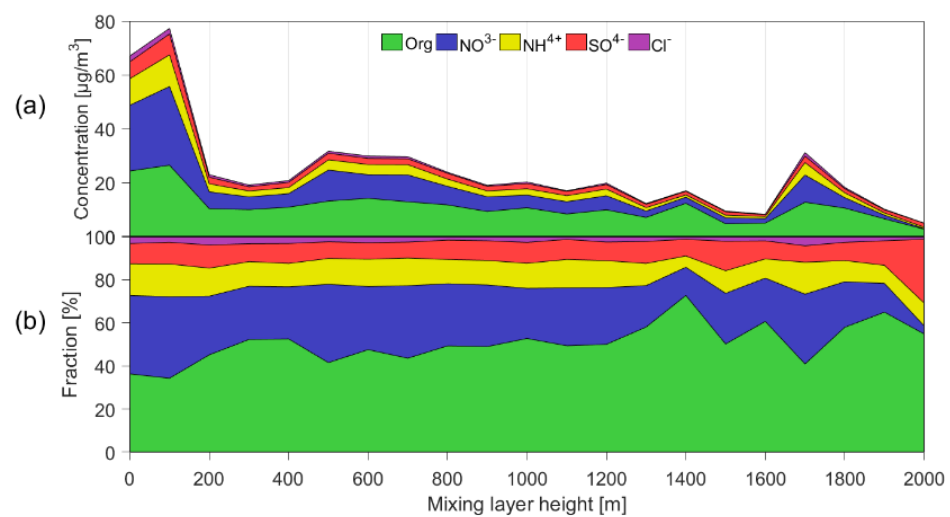
491

492

493

494

495



496

497 Figure 4. Statistical relationship between MLH and concentration (a) and fraction (b) of chemical

498 composition species. Only daytime conditions determined by ceilometer from non-rainy periods

499 (RH<95%) during the observation (~ 6 months) are considered.

500

501

502

503

504

505

506

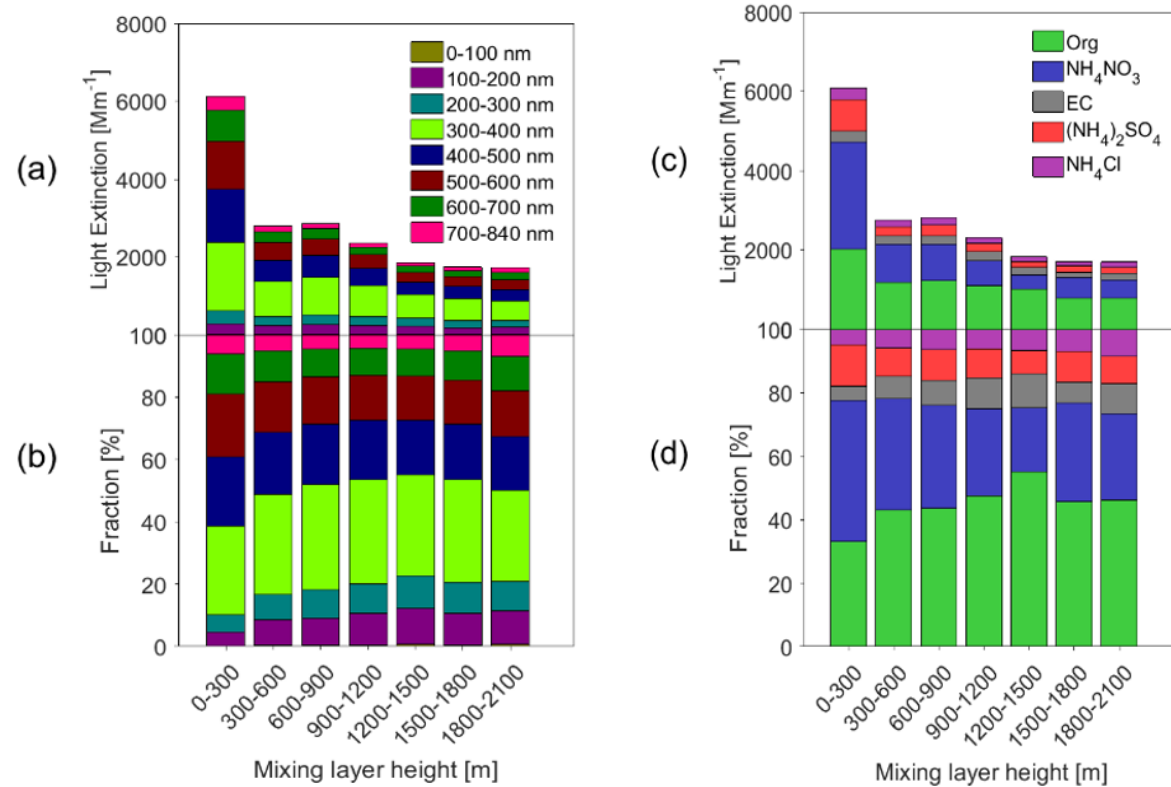
507

508

509

510

511



512

513

514

515

516

517

518

519 Figure 5. Statistical relationship between MLH and light extinction of different aerosol species.

520 Only daytime conditions determined by the ceilometer from non-rainy periods (RH<95%) are

521 considered.

522

523

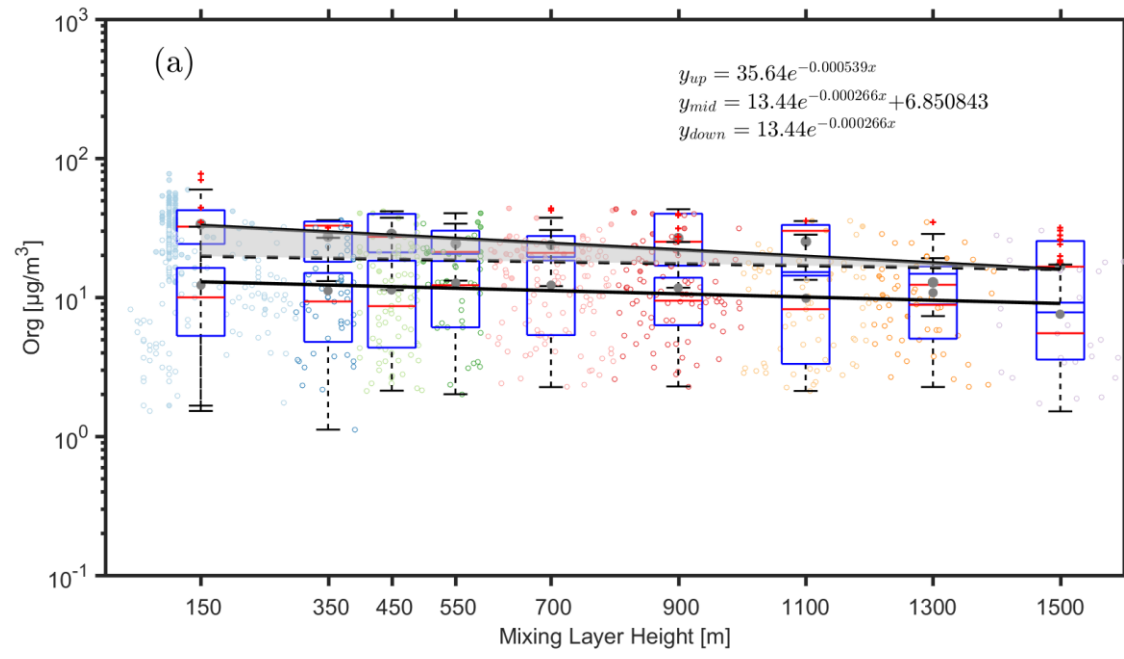
524

525

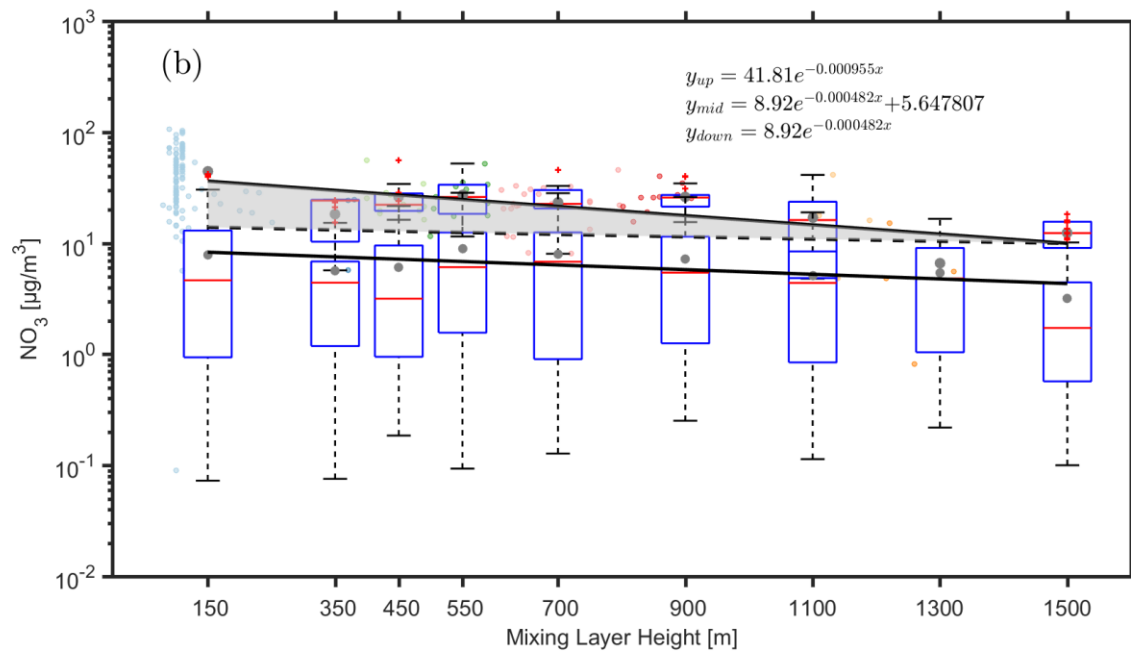
526

527

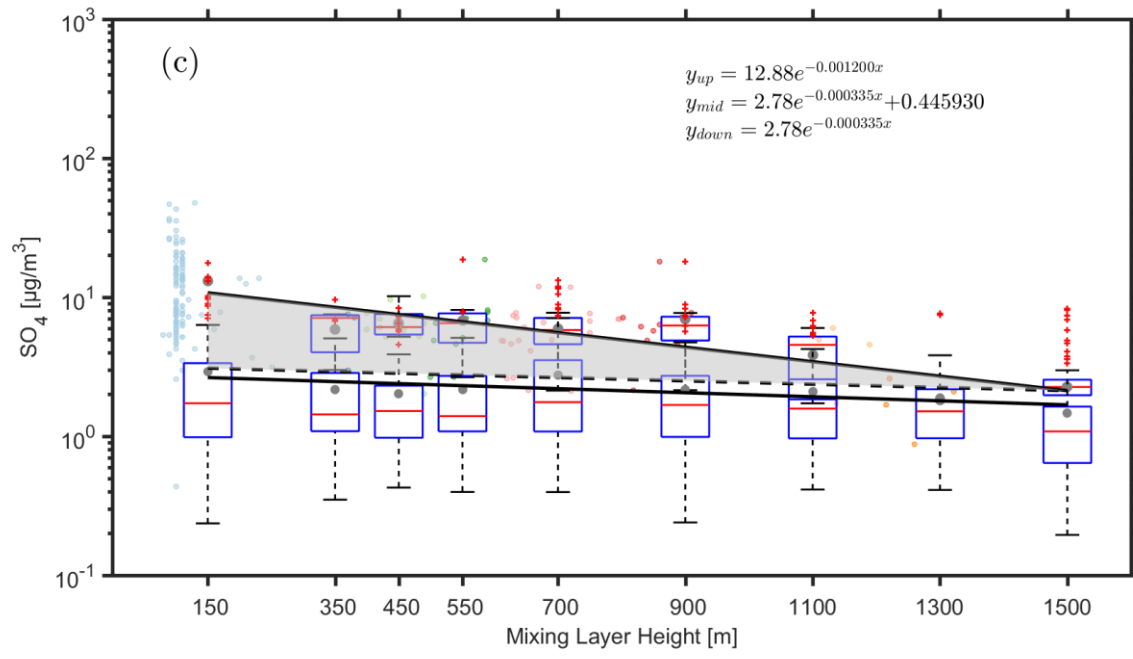
528



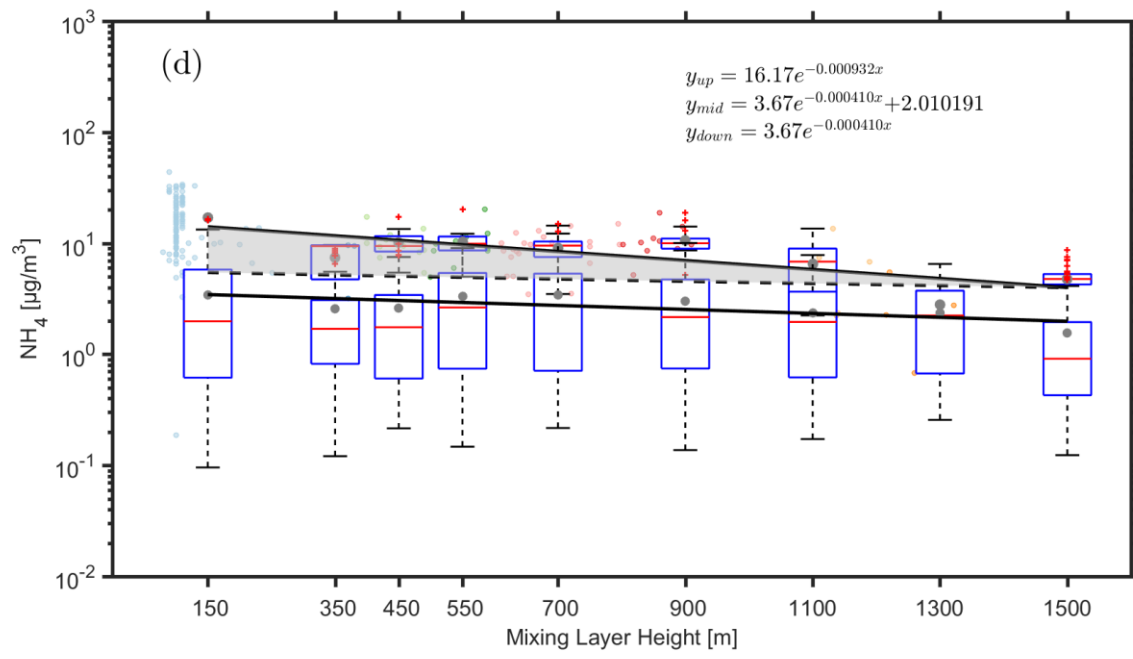
529



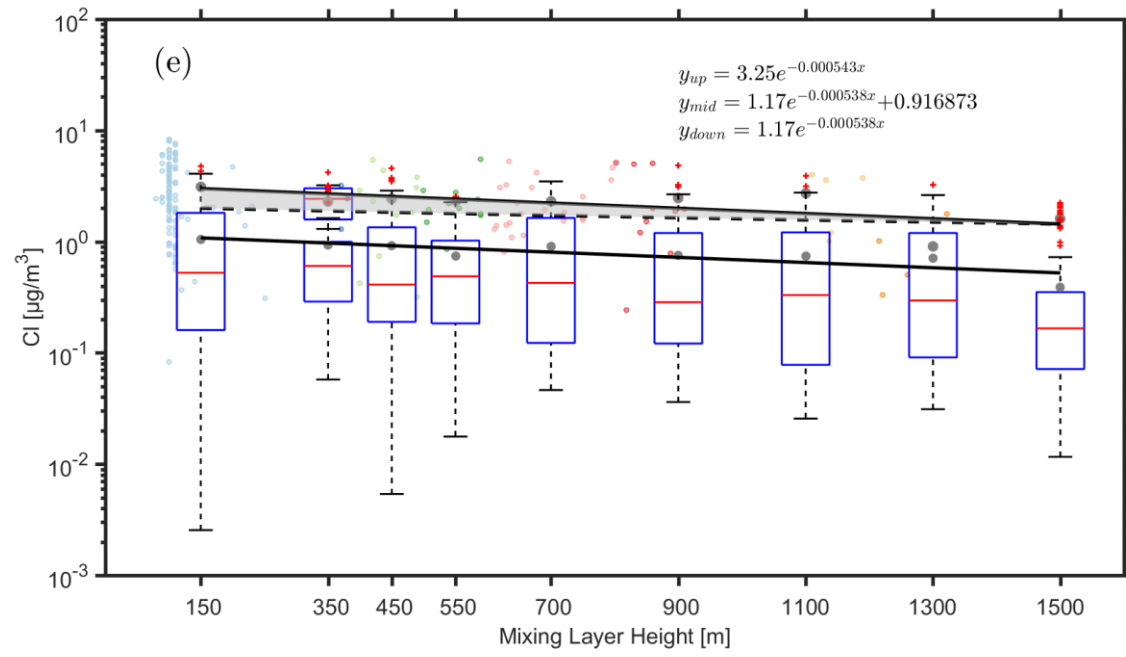
530



531

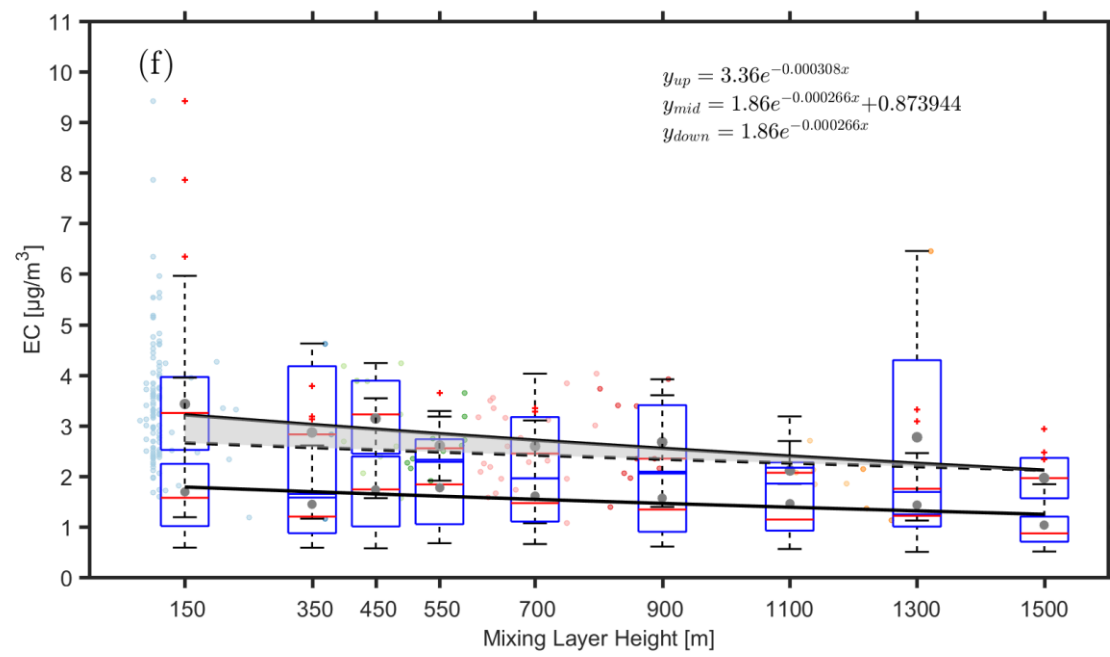


532

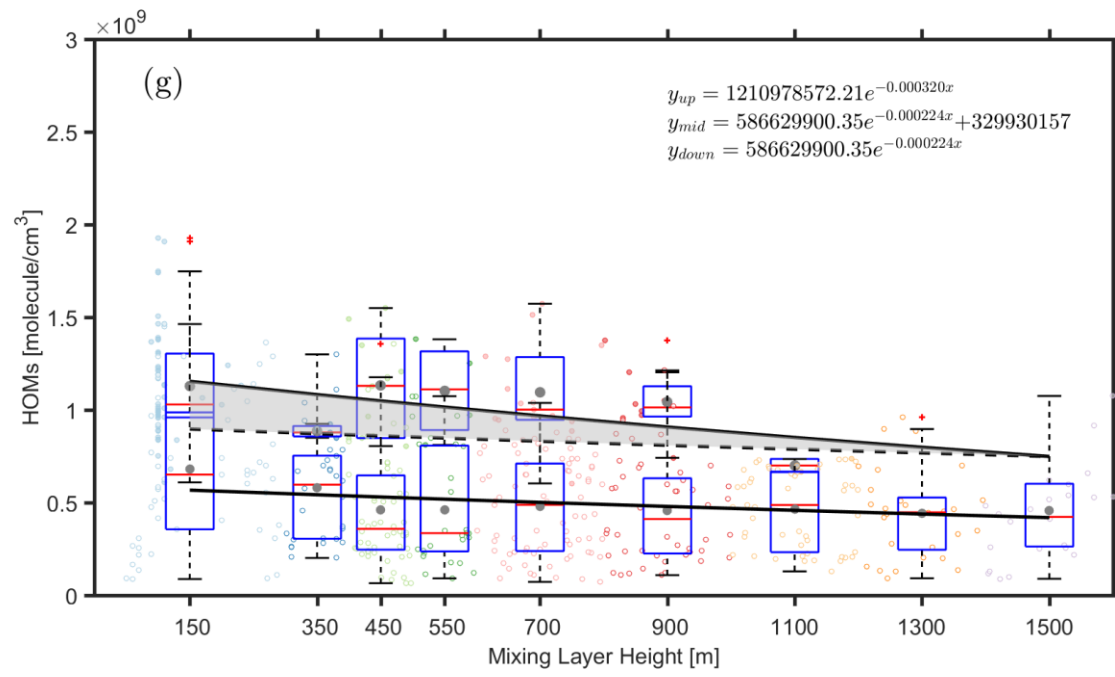


533

534

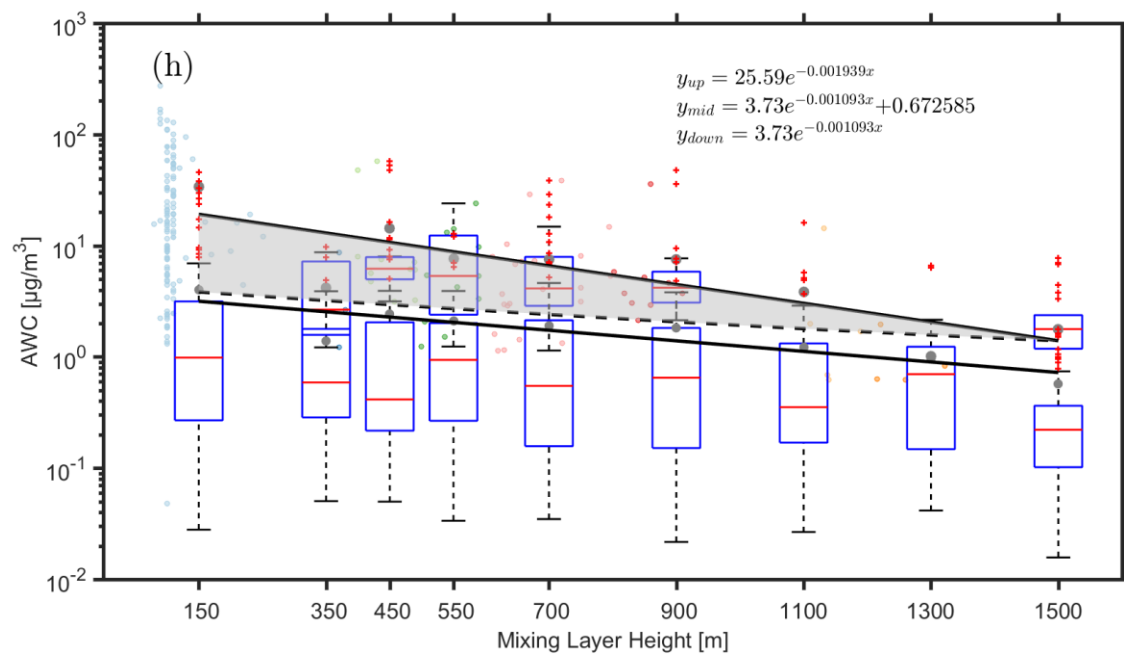


535

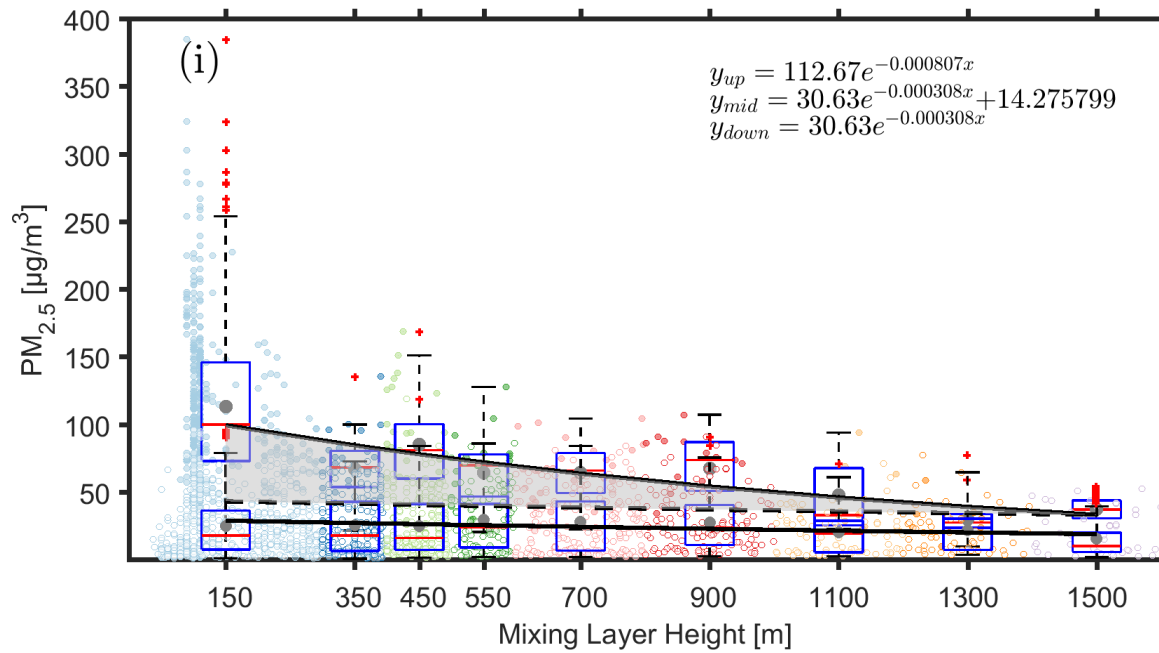


536

537



538



539

540

541 Figure 6. Observed dependency of (organics (a), nitrate (b), ammonium (c), sulfate (d), chlorine (e),
 542 element carbon (f), HOMs (g), AWC (h) and PM_{2.5}(i) on the MLH during polluted and less-polluted
 543 conditions. The data related to the upper fitting line represents PM_{2.5} concentrations larger than 75
 544 µg m⁻³, while the data related to the lower fitting line represents PM_{2.5} concentrations lower than 75
 545 µg m⁻³. Only daytime conditions determined by the ceilometer from non-rainy periods (RH<95%)
 546 were considered. The solid cycles and hollow cycles denotes concentrations that are more than 75
 547 µg m⁻³ and less than 75 µg m⁻³, respectively. The dark grey points and red lines in the boxes
 548 represent mean and median values, respectively. The shaded area between the upper solid and
 549 dotted lines corresponds to an increased amount of the specific compounds with decreased MLH,
 550 assuming that the compound has the same variation pattern under highly- polluted conditions as in
 551 less polluted time.

552

553

554

555

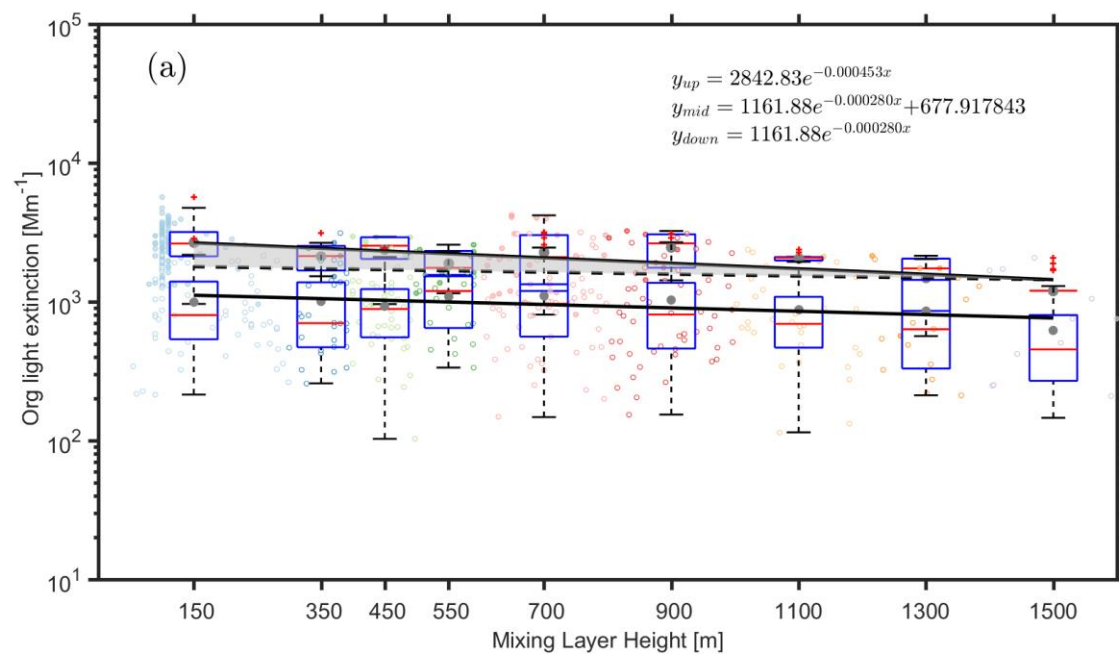
556

557

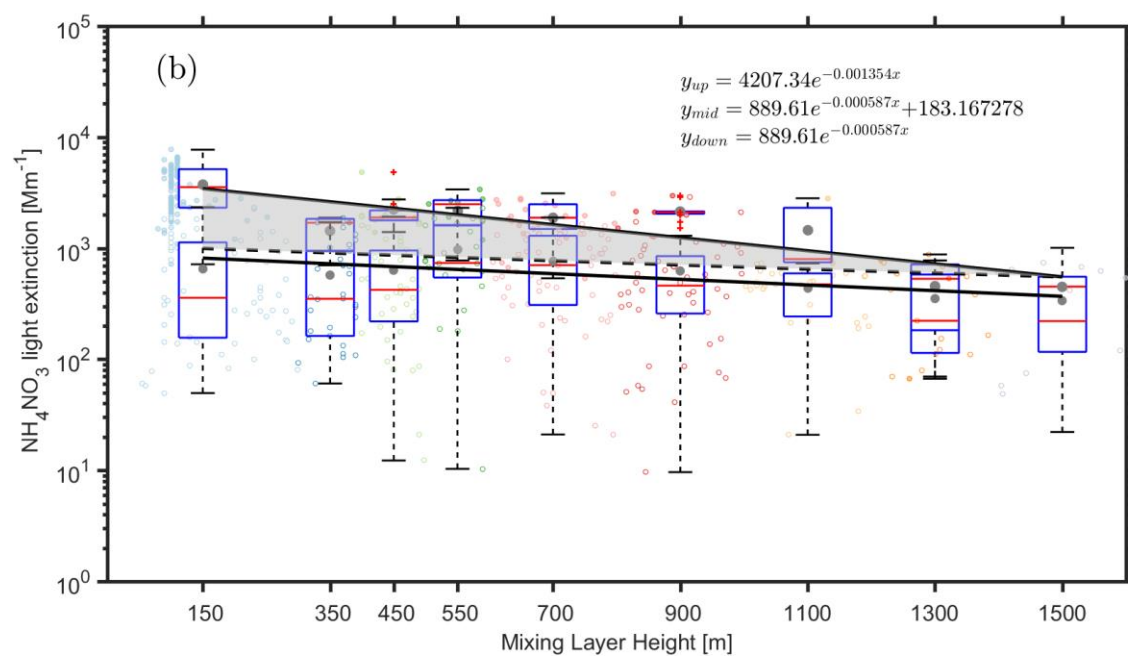
558

559

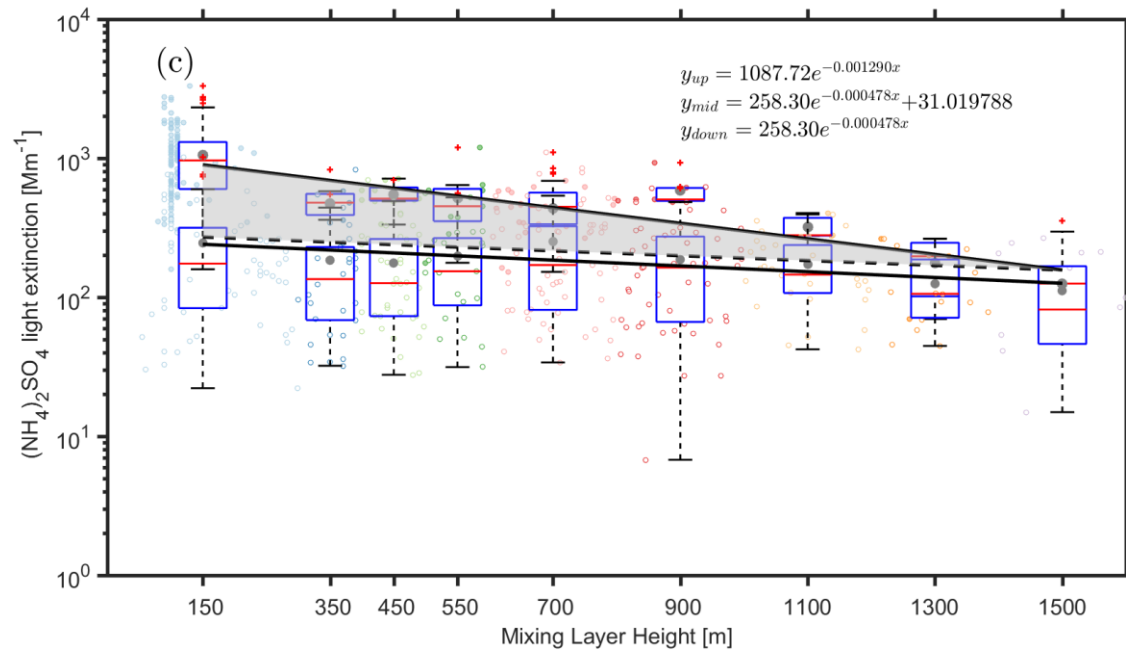
560



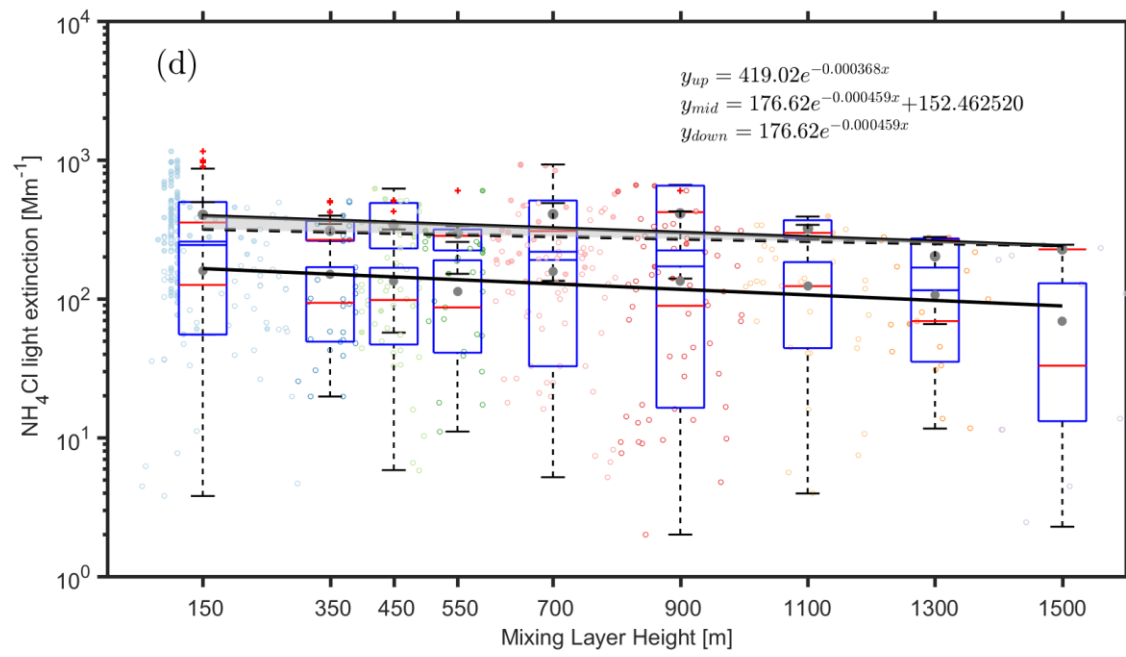
561



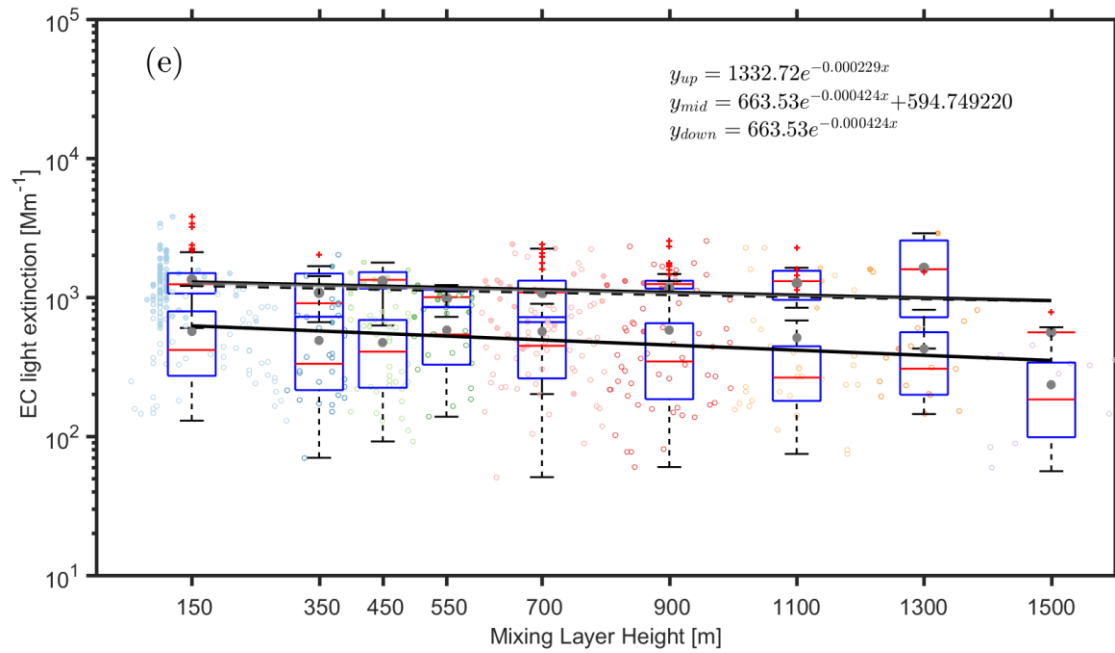
562



563



564



565

566

567

568 Figure 7. Observed dependency of the aerosol light extinction due to NH_4NO_3 (a) $(\text{NH}_4)_2\text{SO}_4$ (b),
 569 NH_4Cl (c) Org (d) and EC (e) on the MLH during polluted and non-polluted conditions. The data
 570 related to the upper fitting line represents $\text{PM}_{2.5}$ concentrations larger than $75 \mu\text{g m}^{-3}$, while the data
 571 related to the lower fitting line represents $\text{PM}_{2.5}$ concentrations less than $75 \mu\text{g m}^{-3}$. Only daytime
 572 conditions determined by ceilometer from non-rainy periods ($\text{RH} < 95\%$) are considered. The dark
 573 grey points and red lines in the boxes represent mean and median values, respectively. The shaded
 574 area between the upper solid and dashed line corresponds to an increased amount of $\text{PM}_{2.5}$ with a
 575 decreased MLH, assuming that $\text{PM}_{2.5}$ has the same variation pattern under highly- polluted
 576 conditions as in less polluted time

577

578

579

580

581

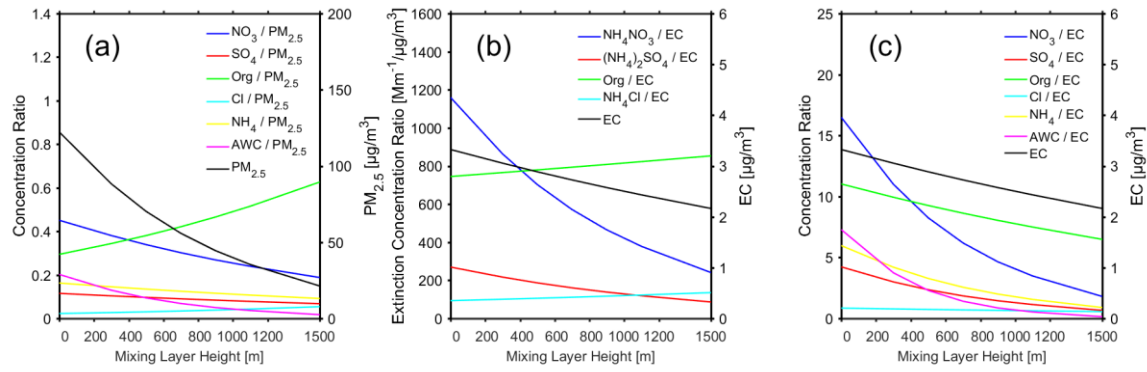
582

583

584

585

586



587

588 Figure 8. (a) the ratio of the mass concentration of different chemical components (nitrate, sulfate,
 589 organics, chlorine, ammonium) and AWC to the mass concentration of $NR_PM_{2.5}$ as a function of
 590 MLH. (b) the ratio of dry aerosol light extinction by different chemical components (NH_4NO_3 ,
 591 $(NH_4)_2SO_4$, Org, NH_4Cl) to the mass concentration EC as a function of MLH (c) the ratio of the
 592 mass concentration of different chemical components (nitrate, sulfate, organics, chlorine,
 593 ammonium) and AWC to the mass concentration of EC as a function of MLH. All the data
 594 corresponds to polluted conditions ($\text{fine PM} > 75 \mu g m^{-3}$), and only daytime conditions determined
 595 by the ceilometer from non-rainy periods ($RH < 95\%$) were considered.

596

597

598

599

600

601

602

603

604

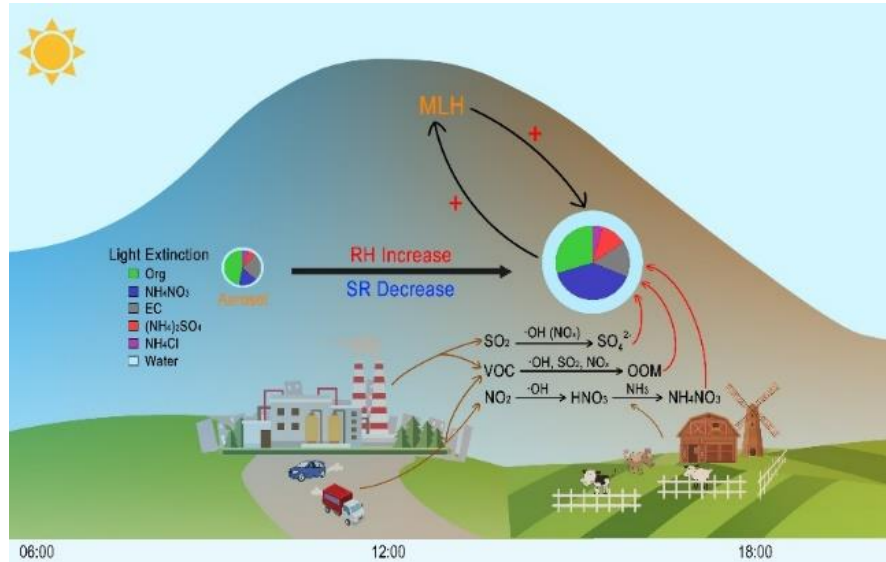
605

606

607

608

609



610

611 **Figure 9. A schematic picture illustrating the process of rapid aerosol mass growth and**
612 **enhanced light extinction in Beijing.** The plus symbols represent the strengthening of a specific
613 process. At the presence of aerosols during afternoon time in Beijing, the intensity of solar radiation
614 reaching the surface will be decreased and relative humidity will be increased. As a result, the
615 development of boundary layer will be suppressed, and the concentrations of aerosol precursors
616 (e.g., SO_2 , NO_2 , VOC) will be increased. In turn, the secondary production of these sulfate, nitrate
617 and oxygenated organic compounds will be enhanced due to increased concentrations and
618 partitioning of these compounds into the aerosol phase. The increased formation of secondary
619 aerosol mass will reduce solar radiation further and the haze formation increased, as shown in pie
620 charts that the light extinction fraction of aerosol changed from organic to nitrate. Noting that
621 during intensive haze periods, nitrate and its contribution to light extinction contribution increased
622 dramatically.

623

624

625

626

